

CERN-EP-2026-019
28 January 2026

Measurement of the charged-particle-jet transverse-momentum fraction carried by prompt and non-prompt J/ψ mesons in pp collisions at $\sqrt{s} = 13$ TeV

ALICE Collaboration*

Abstract

The measurement of the transverse-momentum fraction (z^{ch}) carried by prompt and non-prompt J/ψ in charged-particle jets in proton–proton collisions with a center-of-mass energy $\sqrt{s} = 13$ TeV is reported by the ALICE Collaboration at the CERN Large Hadron Collider. The measurement is based on a Transition Radiation Detector triggered data sample corresponding to an integrated luminosity of $\mathcal{L} = 1.63 \pm 0.03 \text{ pb}^{-1}$. Inclusive J/ψ mesons with transverse momentum (p_{T}) above 1 GeV/ c are reconstructed at midrapidity through the electron–positron decay channel. The prompt and non-prompt J/ψ contributions are separated using the secondary vertices from beauty-hadron decays. Jets are reconstructed from J/ψ -meson candidates and charged particles using the anti- k_{T} algorithm with jet resolution parameter $R = 0.4$ in the pseudorapidity range $|\eta_{\text{jet}}| < 0.5$. The distribution of the charged-particle jet p_{T} fraction carried by the prompt and non-prompt J/ψ mesons, z^{ch} , is measured in the range $0.3 < z^{\text{ch}} \leq 1.0$ for the jet- p_{T} range $7 < p_{\text{T}}^{\text{jet}} < 15$ GeV/ c . The measured z^{ch} distributions for prompt and non-prompt J/ψ are compared to pQCD calculations and PYTHIA 8 simulations. Prompt and non-prompt J/ψ production within charged-particle jets are found to be qualitatively well reproduced by PYTHIA 8 for $z^{\text{ch}} < 0.9$, however, as z^{ch} approaches one, the simulations overshoot the measured data, indicating an overestimation of the fraction of isolated J/ψ . This observed tension between data and simulations in the highest z^{ch} bins reflects the challenge of simulating hadronization of low-momentum jets.

© 2026 CERN for the benefit of the ALICE Collaboration.

Reproduction of this article or parts of it is allowed as specified in the CC-BY-4.0 license.

*See Appendix A for the list of collaboration members

1 Introduction

The production of charmonium states, i.e., the creation of bound states of charm–anticharm quark pairs, is a process which cannot be calculated perturbatively in quantum chromodynamics (QCD), and is therefore a valuable testing ground for QCD-based models [1, 2] attempting to understand hadronization. Charmonium-production models usually couple fixed-order perturbative calculations describing the creation of $c\bar{c}$ pairs with non-perturbative matrix elements describing the evolution into a bound state. Phenomenological approaches, such as the Color Evaporation Model (CEM) [3–5], the Color Singlet Model (CSM) [6], and the non-relativistic QCD (NRQCD) factorization approach [7–9] differ mainly in the description of the charmonium formation process. A set of high-precision cross section and polarization measurements of the lightest charmonium vector state, J/ψ , made at the Large Hadron Collider (LHC) [10–38] have enabled improvements to theoretical descriptions, such as the improved CEM [39, 40] and several NRQCD-based approaches [41–48]. Nevertheless, a universal and successful model of the J/ψ -production mechanism remains elusive, especially in the low transverse-momentum (p_T) range [19, 30, 37].

New observables that correlate charmonium production with hadronic activity in the same event, such as the recent measurement of the hadron yields associated with J/ψ production reported by ALICE in Ref. [38], could help improve our understanding of the formation of the bound state. Studies of J/ψ production in jets – collimated sprays of hadrons resulting from the fragmentation of high- p_T partons – may provide further insight into the production phenomenology. Observables, such as the fraction of jet transverse momentum carried by a J/ψ , are expected to be sensitive to both the perturbative and the non-perturbative aspects of its formation [49]. In particular, the jets where the J/ψ mesons carry most of the jet momentum (isolated J/ψ) are expected to be sensitive to the relative contribution of the hadronization mechanisms via color-singlet and color-octet states leading to J/ψ production.

Measurements of prompt- J/ψ production in jets ($p_T^{\text{jet}} > 20$ GeV/ c) reported by LHCb [50] at forward rapidity in proton–proton (pp) collisions at $\sqrt{s} = 13$ TeV show that the p_T fraction carried by the J/ψ is overestimated by calculations implemented in PYTHIA 8 using the NRQCD framework. Here, prompt J/ψ refers to directly produced J/ψ mesons and feed-down contributions from higher-mass charmonium states. A similar observation was reported by CMS [51] at midrapidity in pp collisions at $\sqrt{s} = 5.02$ TeV for jets with $30 < p_T^{\text{jet}} < 40$ GeV/ c . Likewise, the production of prompt $\psi(2S)$ and $\chi_{c1}(3872)$ in jets reported by LHCb [52] at forward rapidity in pp collisions at $\sqrt{s} = 13$ TeV shows striking differences from PYTHIA 8 predictions for $p_T^{\text{jet}} > 15$ GeV/ c . In this jet- p_T range, the measured distributions indicate two distinct components corresponding to non-isolated and isolated production. The prompt-charmonium production simulated in PYTHIA 8 originates directly from parton–parton interactions. The observed discrepancies may be better described by advanced calculations of charmonium fragmentation functions [53, 54] and the inclusion of a parton shower prior to the J/ψ formation in PYTHIA 8 [55].

In the high jet- p_T regime, the jet production cross section can be determined theoretically using the factorization theorem [56]. In this limit, parton fragmentation is assumed to be universal, i.e., independent of the collision process. However, in the low- p_T range, the factorization may be broken. Measurements of the charm-quark fragmentation fractions show strong deviations from values measured in e^+e^- and ep collisions [57]. Studies of identified particles produced within the jet cone may provide new insights into the hypothesis of universality of parton fragmentation. Recent measurements of charm baryon-tagged jets within a relatively low p_T region ($7 < p_T^{\text{ch jet}} < 15$ GeV/ c) hint at a softer fragmentation into charm baryons with respect to charm mesons [58]. Investigating the fragmentation of J/ψ in jets in a low jet- p_T region may provide complementary input about the fragmentation of heavy quarks (charm and beauty).

The study of in-jet charmonium production in pp collisions is vital for the interpretation of future similar measurements in heavy-ion collisions. At high temperature and close to zero baryon chemical potential, lattice QCD calculations predict a deconfined state of strongly-interacting matter known as the

quark–gluon plasma (QGP) [59, 60]. The charmonium formation process in heavy-ion collisions is complex, with the initial production of heavy-quark pairs predominantly taking place very early in the collision history. The production of bound charmonium states is expected to be strongly affected by the hot medium created in the collision, as the heavy-quark pairs may be subject to effects such as color screening, (re)generation, and parton energy loss [61–64]. In particular, the production of charmonia in ultra-relativistic heavy-ion collisions is one of the most prominent probes of the QGP [61], where phenomenological models differ greatly in the assumed underlying production mechanisms, and accordingly, predicted differential yields. Statistical hadronization models assume that the charm quarks produced in initial hard scatterings reach a complete thermal equilibration in the QGP, and all the bound charmed hadrons are produced at the chemical freeze-out [63, 65]. On the other hand, phenomenological transport models assume that charm hadrons are continuously produced, dissociated, and (re)generated during the entire evolution of the hot and dense matter in the collision zone. [66, 67]. So far, the various models provide a relatively good description of nuclear suppression and azimuthal anisotropy (flow) measurements [68–70], requiring further measurements to distinguish between the assumed underlying production mechanisms. Studies of charmonium-tagged jets and the modification of the jet substructure in heavy-ion collisions may provide a complementary insight into charmonium production, the energy-loss mechanisms of heavy quarks, and the properties of the produced deconfined medium [71, 72].

This paper presents measurements of J/ψ production within charged-particle jets (i.e., jets reconstructed using only charged-particle tracks) in pp collisions at a center-of-mass energy of $\sqrt{s} = 13$ TeV. The measurement is performed using a Transition Radiation Detector (TRD) triggered data sample recorded by the ALICE detector at the LHC, corresponding to an integrated luminosity of $\mathcal{L} = 1.6 \pm 0.03$ pb $^{-1}$. The fraction of the jet transverse momentum carried by the J/ψ , defined as

$$z^{\text{ch}} \equiv \frac{p_{\text{T}}^{J/\psi}}{p_{\text{T}}^{\text{ch jet}}}, \quad (1)$$

is determined separately for prompt and non-prompt J/ψ , where the latter refers to J/ψ mesons originating from the decay of beauty hadrons. Jets are reconstructed using the anti- k_{T} algorithm [73] with a jet resolution parameter of $R = 0.4$. Reconstructed jets are required to be in the pseudorapidity range $|\eta_{\text{jet}}| < 0.5$ and have a p_{T} in the range $7 < p_{\text{T}}^{\text{ch jet}} < 15$ GeV/ c . The reconstruction of J/ψ mesons is done at midrapidity through the electron–positron decay channel for J/ψ with $p_{\text{T}}^{J/\psi} > 1$ GeV/ c and the separation between the prompt and the non-prompt components using the displacement between the primary collision vertex and the J/ψ decay vertex.

2 Detector setup and data samples

A full description of the ALICE setup and detector performance can be found in Refs. [74, 75]. In the following, the detectors employed in this analysis and their roles are described. The Inner Tracking System (ITS) is a six-layer silicon detector located around the beam pipe. The two innermost layers of the ITS barrel are Silicon Pixel Detectors (SPD) with excellent spatial resolution placed at a radial distance of $r = 3.9$ and 7.6 cm from the beam line. This detector is used for primary and secondary-vertex reconstruction, and also for tracking. In particular, the high spatial resolution of the ITS enables the measurement of displaced decay vertices, therefore allowing for the separation between the prompt and non-prompt J/ψ . The Time Projection Chamber (TPC) [76] is a cylindrical gaseous detector covering a radial distance between 85 and 250 cm. It is located around the ITS and extends 250 cm in the longitudinal direction on each side of the nominal interaction point. The TPC is used for tracking and particle identification (PID) based on the specific energy loss of particles interacting with the TPC gas. The TPC and ITS cover the full azimuthal angle and provide tracking and PID performance in the pseudorapidity range $|\eta| < 0.9$. The Transition Radiation Detector (TRD) [77] surrounds the TPC and covers the full azimuthal angle and the pseudorapidity range $|\eta| < 0.84$. The TRD consists of 522 chambers arranged in

Table 1: Overview of the number of selected events and corresponding integrated luminosity in the analyzed data and MC samples.

Trigger	<i>data</i>		<i>simulation</i>
	MB	TRD	MC, J/ψ injected
Number of events	1.06×10^9	1.71×10^8	7.86×10^7
Integrated luminosity	$17.83 \pm 0.33 \text{ nb}^{-1}$	$1.63 \pm 0.03 \text{ pb}^{-1}$	–

18 sectors in azimuth and in six radial layers and five stacks in the longitudinal direction. Each chamber consists of a fiber mat sandwiched between two foam sheets operating as radiator material, where highly boosted particles emit transition radiation. Behind the radiators, multi-wire proportional drift chambers with pad readout, filled with a Xe–CO₂ gas mixture, provide tracking. In addition, the signals from the drift region provide measurements of the specific energy loss of charged particles and the energy of transition-radiation photons originating from the relativistic electrons crossing the radiator material. Since the tracking and PID signal can be computed online, the TRD is used as an electron trigger, with a decision being issued within 6 μs after the collision time. Two scintillator arrays (V0 detectors) [78] situated along the beam direction at $-3.7 < \eta < -1.7$ and $2.8 < \eta < 5.1$ are used for the minimum-bias triggering and event characterization.

The analysis discussed in this article is based on data recorded in the years 2017 and 2018 in pp collisions with center-of-mass energy $\sqrt{s} = 13$ TeV. The data sample corresponds to events triggered by the TRD using a condition that at least one TRD track, i.e., a track segment measured in the TRD and constrained to the primary vertex, with a particle p_T higher than 2 GeV/ c and a PID signal compatible with the electron hypothesis. To reduce the contribution to electron-triggered events due to photon conversions in the detector material, the trigger condition also requires the track to have five tracklets per stack, including one in the first TRD layer. The background from secondary electrons is further reduced using a selection on the pointing angle of the track [79]. Besides the TRD-triggered data sample, a minimum-bias (MB) data sample is considered to evaluate the TRD-trigger performance in data. MB events are selected based on the coincidence of the signals in the V0 scintillator arrays.

Selected events are required to have a reconstructed primary vertex located within ± 10 cm of the nominal interaction point along the beam direction. With a maximum interaction rate of 260 kHz, the probability for pileup events from the same bunch crossing is 0.5×10^{-3} [30]. An offline algorithm which identifies multiple vertices [75] is used to reject these events. Beam–gas events and collisions from other LHC bunch crossings occurring within the readout time of the SPD are rejected based on offline timing cuts using information from the V0.

A simulated Monte Carlo (MC) sample is used in the determination of probability density functions (PDFs) required for the extraction of the non-prompt J/ψ fraction (described in Sec. 3.2) and for necessary corrections (described in Sec. 3.3). The MC sample consists of MB pp events generated with PYTHIA 6.4 [80], where additional prompt and non-prompt J/ψ mesons are injected. The non-prompt J/ψ mesons originate from the decay of beauty hadrons as implemented in PYTHIA 6, while the prompt J/ψ mesons are simulated with a p_T spectrum based on a phenomenological interpolation of existing cross section measurements [81]. The J/ψ -meson decay is simulated with EvtGen [82] using the PHOTOS model [83], which takes into account the QED radiation at the decay vertex. The generated particles are transported through a simulated ALICE detector setup using GEANT 3 [84], and then reconstructed using the same workflow as for real data. In particular, the TRD trigger is also emulated in the MC simulation by applying the same selection criteria as in data. An overview of the number of selected events and corresponding integrated luminosity for the analyzed data and MC samples is shown in Tab. 1.

3 Analysis

The J/ψ mesons are reconstructed at midrapidity through their electron–positron decay channel. The separation of prompt and non-prompt J/ψ is done on a statistical basis by using the displacement of the reconstructed secondary vertex of the decaying beauty hadron. The jets are reconstructed from charged particles in the central barrel using the anti- k_T algorithm [73]. The following section describes the analysis in detail.

3.1 Track selection

The reconstruction of J/ψ mesons is done by combining electron and positron tracks. The tracks are reconstructed in the central barrel based on information from the ITS and TPC, following the selections used in previous analyses reported in Refs. [18, 79]. Selected tracks are required to be within the TRD acceptance ($|\eta| < 0.84$) with a minimum p_T of 1 GeV/ c . In order to reach a good spatial resolution, needed for the secondary vertexing and to reject background from photon conversions, tracks are required to have at least one hit in the SPD layers. To ensure a good momentum and PID resolution, a minimum of 70 space points in the TPC is also required. In order to further reject secondary electrons, candidates are required to have a maximum distance-of-closest approach (DCA) to the reconstructed collision vertex of 1 cm in the radial direction and 3 cm along the beam axis. Electrons are identified by their specific energy loss measured in the TPC, and are selected to be within a band of $\pm 3\sigma$ relative to the expected electron energy-loss curve, where σ represents the resolution of the energy loss associated with each track. To minimize contamination from protons and pions, electron-candidate tracks compatible with the proton or pion energy loss expectation within 3σ are rejected. In order to increase the J/ψ -reconstruction efficiency at high p_T , a rejection criteria of 2σ is chosen for electron candidates with momentum above 5 GeV/ c .

For the jet reconstruction, a less stringent track selection is applied in order to provide a uniform acceptance in η and ϕ . Charged-particle tracks are required to be within the acceptance of the central barrel ($|\eta| < 0.9$) with a minimum p_T of 0.15 GeV/ c . Jets are reconstructed using the anti- k_T algorithm [73] as implemented in the FastJet package [85] using the p_T scheme for recombination. The jet reconstruction is performed with a jet resolution parameter $R = 0.4$ and a minimum jet $p_T^{\text{ch jet}}$ of 5 GeV/ c . Jets are required to have a pseudorapidity of $|\eta_{\text{jet}}| < 0.5$ to ensure that they stay fully within the detector acceptance. The possible bias introduced by J/ψ decay electrons restricted to the TRD-trigger acceptance while jets are restricted by the central-barrel acceptance was found to be negligible. Jet reconstruction is performed in events where at least one J/ψ candidate is found, where the decay electrons corresponding to a J/ψ candidate are removed before the jet reconstruction and are replaced by the four-momentum of the reconstructed J/ψ candidate. In the rare case of more than one J/ψ candidate in an event, this step is done separately for each J/ψ candidate. After the jet-reconstruction procedure, the fraction of p_T carried by the J/ψ candidate within its jet, z^{ch} , is obtained. No subtraction of the underlying event is applied, since the background in this p_T range is negligible for pp collisions.

3.2 Extraction of the prompt and non-prompt J/ψ yields

The extraction of the J/ψ yields in each z^{ch} interval relies on building the invariant mass of all possible electron–positron pairs from the same event. Additionally, for the separation of the non-prompt J/ψ component, originating from beauty-hadron decays, the secondary vertex for each pair is also constructed. The method consists of a two-dimensional likelihood fit of the invariant-mass ($m_{e^+e^-}$) and pseudo-proper decay-length distribution (x). The pseudo-proper decay length is defined as

$$x = c \times L_{xy}^{J/\psi} \times \frac{M^{J/\psi}}{p_T^{J/\psi}}, \quad (2)$$

where $L_{xy}^{J/\psi}$ represents the transverse projection of the distance between the primary and the secondary vertices, $M^{J/\psi}$ is the world-average value of the J/ψ mass [86], and $p_T^{J/\psi}$ is the transverse momentum of the J/ψ candidate.

The fit procedure maximizes the logarithm of a likelihood function

$$\ln\{\mathcal{L}\} = \sum_{i=1}^N \ln\{f_{\text{Sig}} \times \mathcal{F}_{\text{Sig}}(x) \times \mathcal{M}_{\text{Sig}}(m_{e^+e^-}) + (1 - f_{\text{Sig}}) \times \mathcal{F}_{\text{Bkg}}(x) \times \mathcal{M}_{\text{Bkg}}(m_{e^+e^-})\}, \quad (3)$$

where N is the total number of J/ψ candidates in the invariant-mass range $2.4 < m_{e^+e^-} < 3.6$ GeV/ c^2 . The terms $\mathcal{F}_{\text{Sig}}(x)$ and $\mathcal{F}_{\text{Bkg}}(x)$ represent the probability density functions (PDFs) of the pseudo-proper decay-length distributions for signal and background, respectively. In the same manner, the terms $\mathcal{M}_{\text{Sig}}(m_{e^+e^-})$ and $\mathcal{M}_{\text{Bkg}}(m_{e^+e^-})$ represent the PDFs describing the invariant-mass distributions for signal and background, respectively. The fraction of J/ψ signal within the invariant-mass range defined above is represented by f_{Sig} and is a free parameter of the fit. The PDF describing the pseudo-proper decay-length distribution of the J/ψ signal includes two components

$$\mathcal{F}_{\text{Sig}}(x) = f'_B \times \mathcal{F}_B(x) + (1 - f'_B) \times \mathcal{F}_{\text{prompt}}(x), \quad (4)$$

where $\mathcal{F}_{\text{prompt}}(x)$ and $\mathcal{F}_B(x)$ correspond to the prompt and non-prompt J/ψ, respectively. The term f'_B represents the uncorrected fraction of non-prompt J/ψ and is also a free parameter of the fit. A complete description of the different PDFs entering the maximum-likelihood fit is given in Refs. [21, 87]. In this analysis, the PDFs corresponding to the J/ψ signal, $\mathcal{M}_{\text{Sig}}(m_{e^+e^-})$, $\mathcal{F}_{\text{prompt}}(x)$, and $\mathcal{F}_B(x)$, are obtained based on a MC simulation. Since both the invariant mass and the x PDFs are p_T dependent, a weighted average of each of these PDFs is employed for every considered z^{ch} interval, according to

$$T(z^{\text{ch}}) = \frac{\sum_{p_T} T(p_T^{J/\psi}) \times N_{e^+e^-}(p_T^{J/\psi}; z^{\text{ch}})}{N_{e^+e^-}(z^{\text{ch}})}, \quad (5)$$

where $T(p_T^{J/\psi})$ is a J/ψ signal PDF in a given $p_T^{J/\psi}$ interval, and $N_{e^+e^-}(p_T^{J/\psi}; z^{\text{ch}})$ is the number of electron–positron pairs with transverse momentum $p_T^{J/\psi}$ in the z^{ch} interval of interest.

The PDFs describing the background distributions, $\mathcal{M}_{\text{Bkg}}(m_{e^+e^-})$ and $\mathcal{F}_{\text{Bkg}}(x)$ are determined from data. The invariant-mass distribution of the background is parametrized by a third-order polynomial function for $z^{\text{ch}} < 0.7$ and an exponential for $z^{\text{ch}} > 0.7$. The PDF describing the pseudo-proper decay-length distribution of the background is determined by fitting the distributions in the sideband regions $2.4 < m_{e^+e^-} < 2.6$ GeV/ c^2 and $3.2 < m_{e^+e^-} < 3.6$ GeV/ c^2 with a functional form described in detail in Ref. [21].

Superimposed projections of the total maximum-likelihood fit function on the invariant-mass and pseudo-proper decay-length distributions are shown in Fig. 1 for two different z^{ch} bins. The maximum-likelihood fit is done in bins of z^{ch} for three different jet $p_T^{\text{ch,jet}}$ ranges, further described in section 3.4.

3.3 Acceptance and efficiency corrections

For a given z^{ch} interval, the corrected yields of prompt (N_{prompt}) and non-prompt ($N_{\text{non-prompt}}$) J/ψ are obtained as

$$N_{\text{prompt}} = (1 - f_B) \times N_{\text{inclusive}}, \quad (6)$$

$$N_{\text{non-prompt}} = f_B \times N_{\text{inclusive}}, \quad (7)$$

where $N_{\text{inclusive}}$ and f_B are the corrected number of inclusive J/ψ and the corrected fraction of non-prompt J/ψ, respectively. The corrected number of inclusive J/ψ is obtained as

$$N_{\text{inclusive}} = \frac{N_{\text{inclusive}}^{\text{raw}}}{(\mathcal{A} \times \mathcal{E}) \times \mathcal{E}_{\text{TRD}}}, \quad (8)$$

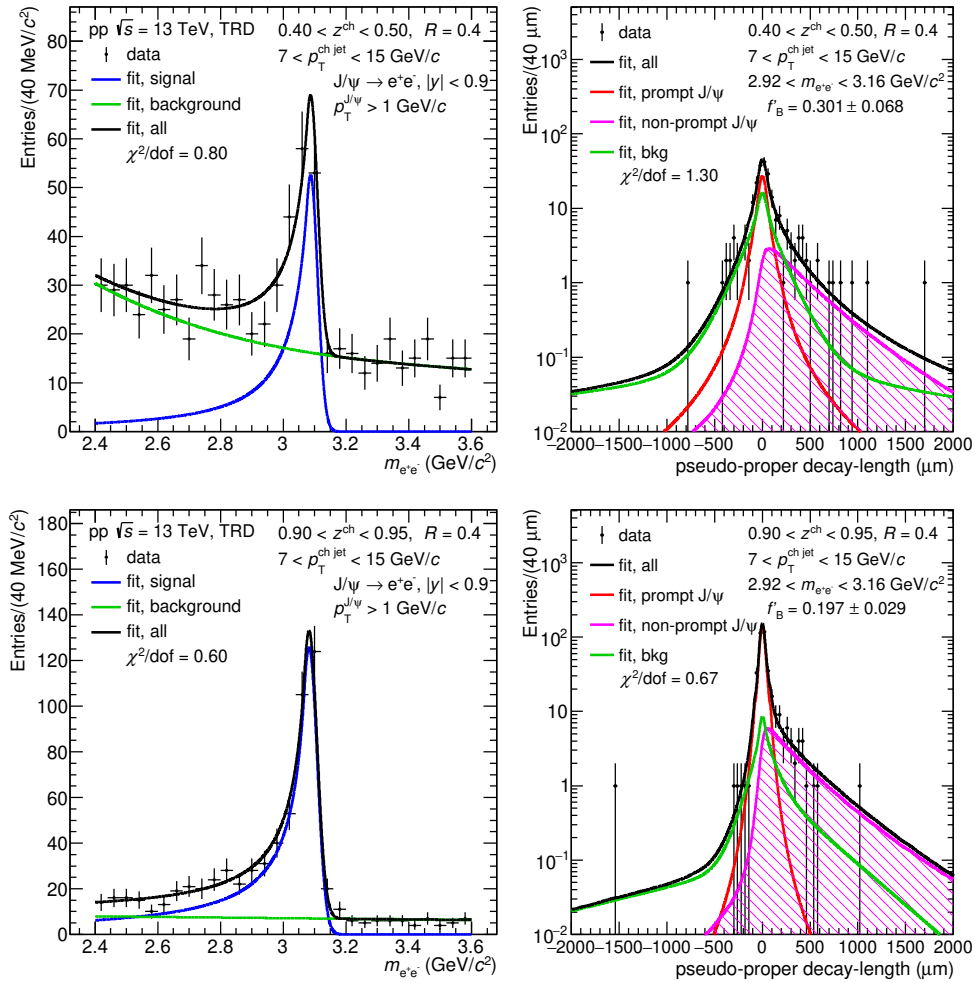


Figure 1: Invariant-mass (*left*) and pseudo-proper decay-length (*right*) distributions for J/ψ candidates, measured in charged-particle jets with $7 < p_T^{\text{ch jet}} < 15$ GeV/c, with superimposed projections of the maximum-likelihood fit for the intervals $0.4 < z^{\text{ch}} < 0.5$ and $0.90 < z^{\text{ch}} < 0.95$ in the top and bottom panels, respectively. The pseudo-proper decay-length distributions are shown for J/ψ candidates reconstructed in the invariant-mass range $2.92 < m_{e^+e^-} < 3.16$ GeV/c² for display purposes only.

where $N_{\text{inclusive}}^{\text{raw}}$ is the number of raw J/ψ -signal counts obtained by summing the invariant-mass distribution after the subtraction of the background distribution resulting from the fit. The $(\mathcal{A} \times \varepsilon)$ is a correction factor obtained from simulations, accounting for the J/ψ kinematic acceptance, the reconstruction efficiency, and the fraction of J/ψ signal found within the invariant-mass window used to count the signal. The TRD trigger efficiency, ε_{TRD} , is determined from simulations following the procedure outlined in Ref. [79]. The algorithm for the TRD trigger is emulated in the MC simulations, where quantities such as the electron likelihood, the online reconstruction of p_T , and the number of track segments per stack are calculated to derive an analogous trigger decision. Figure 2 shows the total acceptance and efficiency, and the corresponding efficiency contributions.

Although for a given $p_T^{J/\psi}$ value, the acceptance times efficiency is the same for prompt and non-prompt J/ψ , when considering finite $p_T^{J/\psi}$ intervals, the average correction factors are slightly different due to the $p_T^{J/\psi}$ dependence of the $(\mathcal{A} \times \varepsilon)$ and the fact that the prompt and non-prompt J/ψ have different $p_T^{J/\psi}$ distributions. This is taken into account by applying a correction to the raw f_B' obtained from the fit to

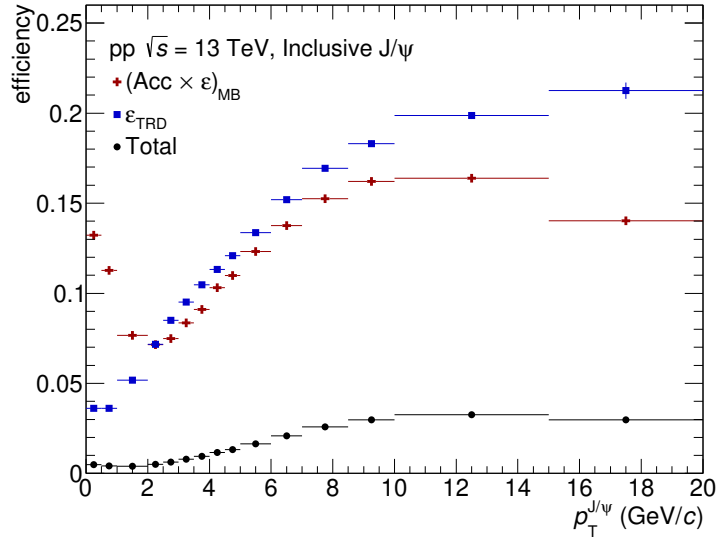


Figure 2: J/ψ acceptance and reconstruction efficiency (red cross), TRD trigger efficiency (blue box), and total efficiency (black point) as a function of transverse momentum.

the data, such that the corrected f_B is obtained as

$$f_B = \left(1 + \frac{1 - f'_B}{f'_B} \times \frac{\langle \mathcal{A} \times \mathcal{E} \rangle_B}{\langle \mathcal{A} \times \mathcal{E} \rangle_{\text{prompt}}} \right)^{-1}, \quad (9)$$

where f'_B is obtained from the fit, and $\langle \mathcal{A} \times \mathcal{E} \rangle_{\text{prompt}}$ and $\langle \mathcal{A} \times \mathcal{E} \rangle_B$ represent the weighted average acceptance and efficiency of the prompt and non-prompt J/ψ in a given z^{ch} range, respectively, obtained following the same weighting procedure as described by Eq. 5. The efficiency-corrected f_B values are in the range 0.15–0.41 for $7 < p_T^{\text{ch jet}} < 15$ GeV/ c .

3.4 Unfolding

A two-dimensional ($z^{\text{ch}}, p_T^{\text{ch jet}}$) Bayesian unfolding procedure [88], as implemented in the RooUnfold package [89], is applied to correct for bin migration due to detector resolution and inefficiencies. The correction is encoded in a 4-dimensional response matrix, which maps the generator-level variables ($z^{\text{ch}}, p_T^{\text{ch jet}}$) to the corresponding detector-level variables. Here, generator-level jets correspond to MC-truth-level charged particles passing the kinematic selections $|\eta| < 0.9$ and $p_T > 0.15$ GeV/ c reconstructed using the jet finding procedure described in Sec. 3.1. The response matrix is populated with generator- and detector-level J/ψ -tagged jets obtained from the MC sample described in Sec. 2. The generator- and detector-level jets are matched by requiring the same J/ψ candidate among the jet constituents. Due to the significantly larger amount of computing required to generate jets with prompt J/ψ with the ALICE Run 2 MC framework, the response matrix is constructed using only non-prompt J/ψ -tagged jets and used to unfold both the prompt and the non-prompt J/ψ z^{ch} distributions. In pp collisions, the charged-track reconstruction performance in the central barrel is independent of the track density and the measurements are therefore not expected to be affected by this choice. Figure 3 shows the projected response matrix, representing the probability of bin migration, where each row of generated bins is normalized to unity.

The unfolded results are reported in the $7 < p_T^{\text{ch jet}} < 15$ GeV/ c and $0.3 < z^{\text{ch}} \leq 1.0$ range. In order to account for migrations below and above these intervals, the response matrix is constructed to cover the p_T interval $5 < p_T^{\text{ch jet}} < 35$ GeV/ c and the z^{ch} interval $0.2 < z^{\text{ch}} \leq 1.0$. Additional residual corrections are applied to account for jets migrating in and out of the response matrix range. The corrections are found

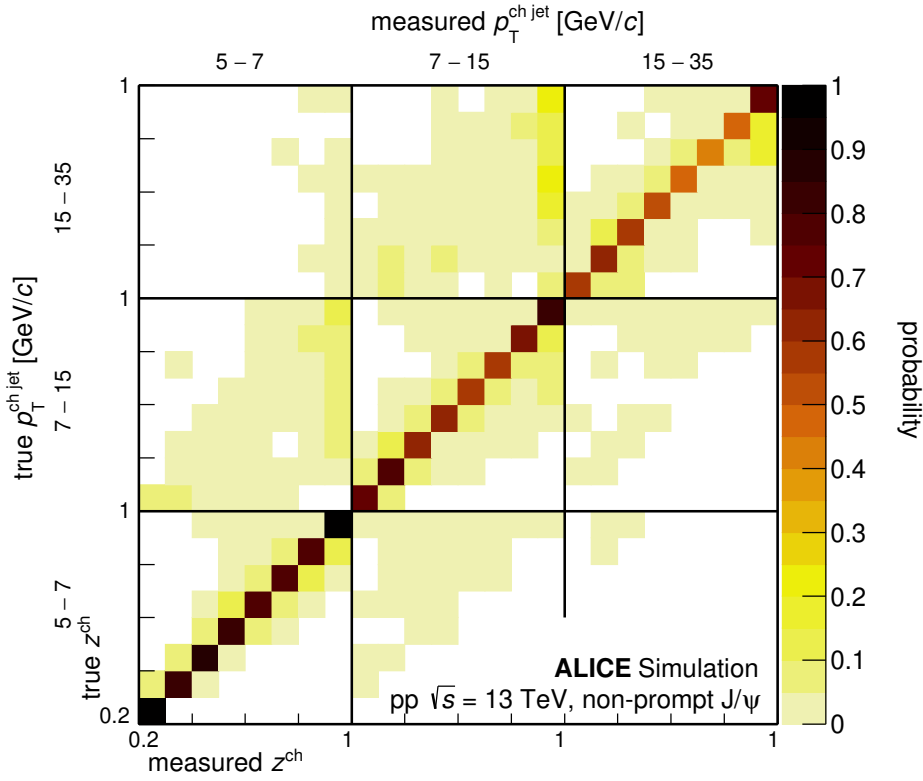


Figure 3: Detector-response matrix for jets containing a non-prompt J/ψ meson, representing the bin-migration probability as a function of the jet $p_T^{\text{ch,jet}}$ and z^{ch} . The y axis represents the true z^{ch} in bins of true $p_T^{\text{ch,jet}}$, and the x axis shows the measured z^{ch} in bins of measured $p_T^{\text{ch,jet}}$.

to be minor.

Several checks are performed to evaluate the stability of the unfolding procedure. Convergence of the unfolding procedure is tested by comparing results of subsequent Bayesian iterations, where convergence is reached after five iterations. This is chosen as the default number of iterations. The unfolding procedure is further tested by refolding the unfolded results and comparing to the measured data. Additionally, a closure test is performed, where the MC sample is split into two independent samples containing 20 and 80% of the statistics. The first sample is used to provide the input distribution for the unfolding procedure, while the second sample is used to construct the response matrix. The closure test assesses how accurately the unfolding of the input spectrum recreates the original MC-generated spectrum. The closure test is performed twice, once with statistical uncertainties on the input spectra provided from the MC distribution and once with statistical uncertainties propagated from the measured distribution in data. In both cases, the ratio between the unfolded and generated distributions fluctuates within a 10% band, with the ratio being statistically compatible with one.

4 Systematic uncertainties

The measurement of J/ψ yields in jet z^{ch} intervals is affected by several independent sources of systematic uncertainties due to electron-candidate selection, J/ψ -signal extraction, separation of prompt and non-prompt J/ψ , TRD trigger efficiency, track-reconstruction efficiency, and unfolding. The evaluation of the different systematic sources follows closely the procedures outlined in Refs. [18, 38, 58, 79].

The systematic uncertainty related to the identification of electron tracks is evaluated by varying the PID selection criteria. Three different PID criteria are investigated, namely a tight and loose hadron (protons

and pions combined) rejection and a tighter electron selection criterion. For each of these variations, the analysis is repeated and the RMS of the considered variations is assigned as the systematic uncertainty. The uncertainty is considered as correlated between z^{ch} bins, and ranges between 1–2% apart from the lowest z^{ch} bin where the uncertainty is about 13%.

The uncertainty on the J/ψ -signal extraction has contributions from both the signal and background fit components. The uncertainty related to the signal component is evaluated by changing the invariant-mass interval in which the J/ψ yield is counted and consequently the correction on the fraction of the yield being counted. Five variations are considered, changing the lower bound by $-80 \text{ MeV}/c^2$ and the upper bound by $\pm 40 \text{ MeV}/c^2$. The uncertainty on the signal component is considered as uncorrelated between z^{ch} bins and ranges from 1–8%, where the uncertainty is largest for the lowest z^{ch} bin. The systematic uncertainty related to the background PDF of the invariant mass is determined by varying the fit function to either a second-order polynomial or an exponential (third-order polynomial for $z^{\text{ch}} > 0.7$). In addition, the upper and lower bounds of the background fit range are varied by $\pm 100 \text{ MeV}/c^2$. The RMS of the variations of the fit function and fit range is assigned as the systematic uncertainty, and ranges from 1–3%.

The systematic uncertainty of the TRD trigger efficiency is evaluated by varying the threshold of the electron and positron likelihood value for the trigger decision. The variation corresponds to the granularity with which the electron/positron likelihood is calculated in the front-end electronics. For each variation, the TRD trigger efficiency is recalculated and used to compute the z^{ch} -dependent J/ψ yields. The RMS of the deviation from the default case is found to be less than 1%. The systematic uncertainty of the TRD trigger efficiency is treated as correlated between the z^{ch} bins.

The systematic uncertainty on the separated prompt and non-prompt J/ψ yields is determined from the uncertainty on the pseudo-proper decay-length PDFs for the background, prompt, and non-prompt J/ψ . The procedure to extract these uncertainties is similar to that performed in previous pp analyses reported in Refs. [18, 21], which includes a plausible modification of the resolution function, changes in the non-prompt input template, and a change in the computation of the primary vertex. In addition, the impact of the input spectrum's p_T shape for prompt J/ψ in the MC is evaluated. The uncertainties related to the prompt and non-prompt pseudo-proper decay-length PDFs are considered to be correlated and range from 1–6%, where the uncertainty decreases for increasing z^{ch} bins.

The systematic uncertainty related to the background fit of the pseudo-proper decay-length distribution is determined by varying the upper and lower sideband regions in steps of ± 50 and $\pm 100 \text{ MeV}/c^2$. The RMS of the considered variations is assigned as the systematic uncertainty related to the pseudo-proper decay-length background PDF. The uncertainty is considered as uncorrelated between the different z^{ch} intervals and ranges from 1–6%, apart from the lowest z^{ch} bin where the uncertainty is 11%.

The systematic-uncertainty contribution from unfolding is estimated by varying the default MC generator-level prior distribution to a flat z^{ch} distribution. Additionally, the default number of five iterations is varied by ± 1 . The RMS of the considered variations is assigned as the systematic uncertainty related to the unfolding procedure, where the uncertainty is considered as uncorrelated between z^{ch} bins. The uncertainties range from 1–10% and 0.3–7% for the prompt and non-prompt J/ψ , respectively. The reconstruction efficiency of tracks used for jet reconstruction is known with 4% uncertainty [58, 90, 91]. Since this efficiency affects the jet-momentum resolution, the corresponding impact of this uncertainty on the measured J/ψ yield in z^{ch} intervals is quantified by repeating the unfolding procedure with a new response matrix where 4% of the tracks are randomly rejected. The systematic uncertainty for a 4% worse tracking efficiency is considered symmetric, accounting also for a 4% increased tracking efficiency. The difference between the unfolded distribution using the default and modified response matrix is assigned as the systematic uncertainty. The uncertainties range from 0.1–10% and 1–11% for the prompt and non-prompt J/ψ , respectively.

Table 2: Summary of systematic-uncertainty contributions for the fraction of transverse momentum carried by prompt and non-prompt J/ψ in charged jets. Uncertainties are listed in percentages. For most bins, the highest uncertainties correspond to the lowest z^{ch} bin, see text for details.

Source	Systematic uncertainty [%]	
	Prompt J/ψ	Non-prompt J/ψ
Electron selection	0.7 – 13.6	
Invariant-mass J/ψ PDF	0.7 – 8.1	
Invariant-mass bkg. PDF	1.3 – 3.1	
x prompt and non-prompt J/ψ PDFs	1.3 – 5.7	
x bkg. PDF	1.4 – 11.4	
TRD trigger efficiency	1.0	
Jet unfolding procedure	0.7 – 10.3	0.3 – 6.5
Tracking efficiency	0.1 – 10.2	1.4 – 11.2
Total	4.1 – 25.1	4.1 – 23.4

The systematic uncertainties are summarized in Tab. 2. The total uncertainties are determined as the sum of the different contributions added in quadrature.

5 Results

The corrected per-jet J/ψ yield distribution, $1/N_{\text{ch jets}}(dN/dz^{\text{ch}})$, as a function of the fraction of jet transverse momentum carried by the J/ψ , z^{ch} , measured for charged-particle jets in the interval $7 < p_{\text{T}}^{\text{ch jet}} < 15$ GeV/ c and for $p_{\text{T}}^{J/\psi} > 1$ GeV/ c , is shown in Fig. 4 for the prompt (left panel) and non-prompt (right panel) components. The prompt- J/ψ distribution exhibits an increasing trend for increasing z^{ch} , with a clear peak as z^{ch} approaches one. The distinct component for $z^{\text{ch}} \approx 1$ is consistent with isolated J/ψ production, indicating that this is the dominant production mechanism in the low $p_{\text{T}}^{\text{ch jet}}$ range. A qualitatively similar observation was also reported recently by the LHCb collaboration in Ref. [52] for prompt $\psi(2S)$ reconstructed in full jets, where the distributions in the low- $p_{\text{T}}^{\text{jet}}$ ranges ($8 < p_{\text{T}}^{\text{jet}} < 11$ GeV/ c and $11 < p_{\text{T}}^{\text{jet}} < 15$ GeV/ c) show a distinct and growing fraction. With increasing $p_{\text{T}}^{\text{jet}}$, the prompt- $\psi(2S)$ distributions reported by the LHCb collaboration show a distinct fraction of non-isolated production in addition to the isolated production, where the evolution of the non-isolated component is shown to be driven by the J/ψ - p_{T} component in each jet- p_{T} interval. The distribution corresponding to the non-prompt J/ψ in charged-particle jets, as shown in the right panel of Fig. 4, is compatible with a rising trend within the current uncertainties. As non-prompt J/ψ originate from the decay of beauty hadrons, it is expected that the non-prompt J/ψ are produced with a larger fraction of surrounding decay products.

The prompt and non-prompt J/ψ z^{ch} distributions are compared to PYTHIA 8.311 simulations using the Monash 2013 tune [92] with two different production settings. In the `softQCD` production setting, prompt- J/ψ production is determined from fixed-order NRQCD calculations directly in the parton-parton scatterings, while the `charmoniumShower` setting allows J/ψ production within a parton shower [55]. The PYTHIA 8 distributions are normalized to unity in the range $0.3 < z^{\text{ch}} \leq 1$, similarly to data. For the prompt J/ψ , the PYTHIA 8 simulations with both settings qualitatively reproduce the rising trend observed in data, however, the z^{ch} distribution is significantly above the measurement in the highest z^{ch} interval, indicating that the fraction of isolated J/ψ is overestimated. A similar trend of the simulation results is observed also for the non-prompt J/ψ , with a good compatibility to data up to $z^{\text{ch}} = 0.9$. For $z^{\text{ch}} > 0.9$, the PYTHIA 8 results exhibit a pronounced peak, not observed in data. Previous measurements of the non-prompt charmonium are well reproduced by PYTHIA 8 simulations [50, 52], where the distributions are peaked around intermediate z values. As non-prompt J/ψ originate from the decay of beauty hadrons, it is expected that the J/ψ is accompanied by other decay products and will thus, cluster into a jet. This would then lead to a larger fraction of non-isolated J/ψ production, as seen

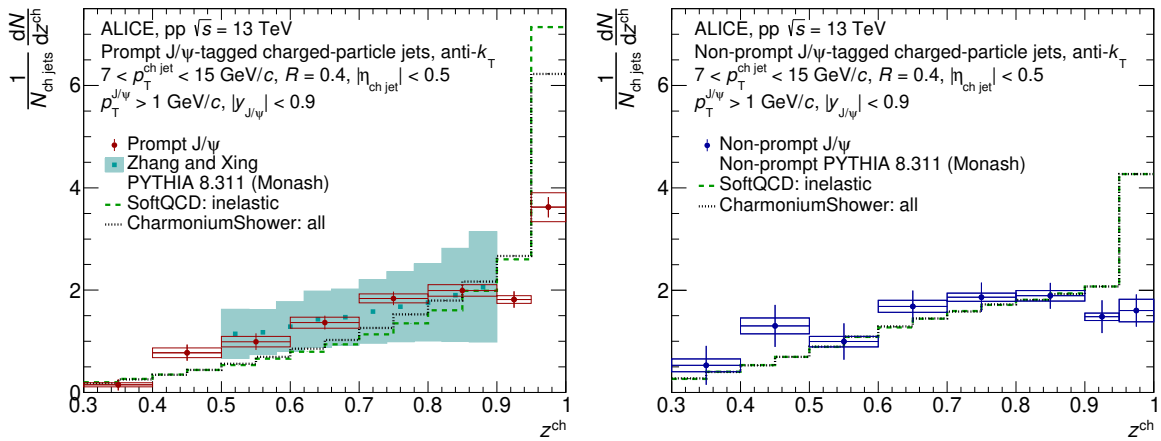


Figure 4: Fully corrected, normalized prompt (*left*) and non-prompt (*right*) J/ψ transverse-momentum fraction (z^{ch}) measured in jets with $7 < p_{\text{T}}^{\text{ch jet}} < 15$ GeV/c for $p_{\text{T}}^{J/\psi} > 1$ GeV/c in pp collisions at $\sqrt{s} = 13$ TeV. Measurements are compared to PYTHIA 8.311 calculations obtained using the Monash 2013 tune [92], where J/ψ are produced directly in parton–parton scatterings (black dotted line) and as a part of a parton shower (green dashed line) [55]. The prompt- J/ψ distribution is compared to a model calculation from Zhang and Xing [93, 94] (cyan box). The error bars represent statistical uncertainties, while the boxes around the data points represent the total systematic uncertainty.

in data. The measurements presented by the LHCb collaboration cover a different phase-space region, as both the jet radius and $p_{\text{T}}^{\text{jet}}$ are larger than for the measurement presented here. With increasing jet radius, one would expect less isolated- J/ψ production, as more surrounding particles, including decay products, are included in the jet, shifting the distribution to lower z values. However, the possible tension between data and simulations in the highest z^{ch} bins may reflect the challenge of simulating hadronization of low-momentum jets.

The left panel of Fig. 4 shows the prompt J/ψ z^{ch} distribution compared to a model calculation from Zhang and Xing [93, 94]. In this calculation, the differential cross section of a parton distribution in a jet is simulated using MadGraph [95] for the creation of the hard parton and using PYTHIA 8 for the parton shower down to the scale of two times the charm mass. The short-distance coefficients, which embody the perturbative part of the calculation, are taken from Ma et al. [96], while the non-perturbative part is represented by long-distance matrix elements (LDMEs) taken from Bodwin et al. [44]. These calculations cover the range $0.5 < z^{\text{ch}} < 0.9$ and in order to compare them to the data, they are normalized such that they match the integral of the measurement in the range $0.5 < z^{\text{ch}} < 0.9$. A very good compatibility with the data is observed, although the theoretical calculations have very large uncertainties, which come from the uncertainty on the LDMEs.

Figure 5 shows the distribution of the fraction of transverse momentum carried by prompt J/ψ in charged-particle jets with $7 < p_{\text{T}}^{\text{ch jet}} < 15$ GeV/c, $|\eta_{\text{jet}}| < 0.5$, and $R = 0.4$ obtained in this analysis in pp collisions at $\sqrt{s} = 13$ TeV compared to the results obtained using full jets with $30 < p_{\text{T}}^{\text{jet}} < 40$ GeV/c, $|\eta_{\text{jet}}| < 2$, and $R = 0.3$ in pp collisions at $\sqrt{s} = 5.02$ TeV reported by CMS in Ref. [51]. The distribution measured by CMS peaks at a z value in the range $0.5 - 0.6$, and does not exhibit an isolated- J/ψ peak at large z . The difference between the ALICE and CMS data seen in Fig 5 is expected to be, in the first order, caused by the different kinematic regions. The recent measurement of prompt $\psi(2S)$ reported by the LHCb collaboration [52] supports this, where the transverse-momentum fraction evolves with jet p_{T} from a shape resembling the prompt- J/ψ ALICE measurement to one more similar to the reported CMS results. In addition, the CMS measurement uses full jets, while in the ALICE measurement charged-particle jets were used, meaning that approximately one third of the jet energy is missing in the case of

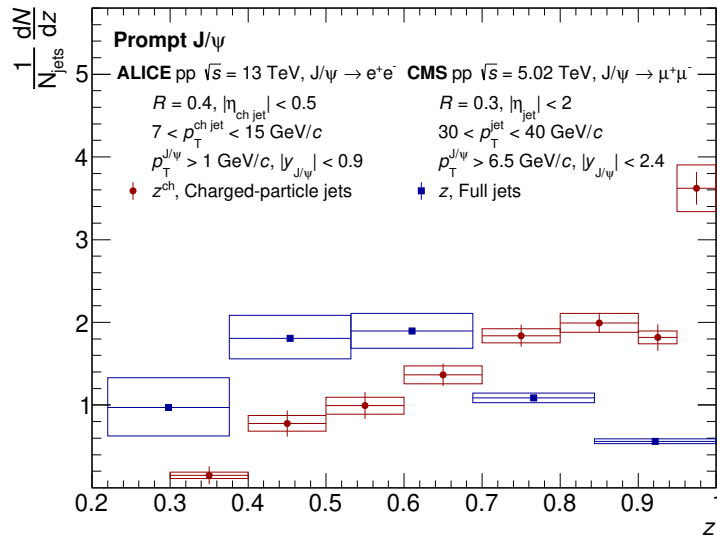


Figure 5: Comparison of the measured prompt J/ψ transverse-momentum fraction (z^{ch}) measured in charged-particle jets with $7 < p_T^{\text{ch,jet}} < 15$ GeV/c for $p_T^{J/\psi} > 1$ GeV/c in pp collisions at $\sqrt{s} = 13$ TeV (red point) with the prompt- J/ψ transverse-momentum fraction (z) measured in full jets with $30 < p_T^{\text{jet}} < 40$ GeV/c for $p_T^{J/\psi} > 6.5$ GeV/c in pp collisions at $\sqrt{s} = 5.02$ TeV reported by CMS (blue box) [51]. The error bars represent statistical uncertainties, while the boxes around the data points represent the total systematic uncertainty.

the charged-particle jets, leading to z^{ch} distributions shifted towards higher z .

6 Summary

This paper presents results on the production of prompt and non-prompt J/ψ mesons in charged-particle jets using data from pp collisions at $\sqrt{s} = 13$ TeV recorded by the ALICE detector at the CERN LHC. The data sample is triggered based on information from the Transition Radiation Detector. The distribution of the transverse-momentum fraction for prompt and non-prompt J/ψ in charged-particle jets is reported for jets with $7 < p_T^{\text{ch,jet}} < 15$ GeV/c, $|\eta_{\text{jet}}| < 0.5$, and resolution parameter $R = 0.4$. The J/ψ candidates are reconstructed at midrapidity through the electron–positron decay channel for J/ψ with $p_T^{J/\psi} > 1$ GeV/c.

The presented measurement is provided in a unique kinematic range at the LHC, investigating for the first time J/ψ production in charged-particle jets at very low jet p_T , sensitive to potential factorization-breaking effects. Both the ALICE results on the prompt and non-prompt J/ψ production within charged-particle jets are found to be qualitatively well reproduced by PYTHIA 8.311 simulations for $z^{\text{ch}} < 0.9$. As z^{ch} approaches one, the simulations overshoot the measured data, which indicates an overestimation of the fraction of isolated J/ψ . The possible tension may also reflect the challenge of simulating hadronization of low-momentum jets. The trend of the prompt- J/ψ distribution can also be described by a pQCD calculation for charmonium fragmentation in the range $0.5 < z^{\text{ch}} < 0.9$. Although the measurements are from different kinematic regions, it is noteworthy that the LHCb results for prompt $\psi(2S)$ are in qualitative agreement with the prompt- J/ψ measurements in the same jet- p_T range [52], and gradually evolve with jet p_T to a shape resembling the reported CMS results of prompt J/ψ at significantly higher jet p_T .

By exploiting the much larger datasets collected by ALICE during the LHC Run 3 and 4, more differential results are expected in the near future. This will give the possibility of further investigating the kinematic dependencies of the J/ψ z^{ch} distributions. Foreseen measurements of the prompt and non-prompt J/ψ production in jets in heavy-ion collisions are expected to provide further information on the

energy-loss mechanisms of heavy quarks in the medium.

Acknowledgements

The ALICE Collaboration would like to thank all its engineers and technicians for their invaluable contributions to the construction of the experiment and the CERN accelerator teams for the outstanding performance of the LHC complex. The ALICE Collaboration gratefully acknowledges the resources and support provided by all Grid centres and the Worldwide LHC Computing Grid (WLCG) collaboration. The ALICE Collaboration acknowledges the following funding agencies for their support in building and running the ALICE detector: A. I. Alikhanyan National Science Laboratory (Yerevan Physics Institute) Foundation (ANSL), State Committee of Science and World Federation of Scientists (WFS), Armenia; Austrian Academy of Sciences, Austrian Science Fund (FWF): [M 2467-N36] and Nationalstiftung für Forschung, Technologie und Entwicklung, Austria; Ministry of Communications and High Technologies, National Nuclear Research Center, Azerbaijan; Rede Nacional de Física de Altas Energias (Renafae), Financiadora de Estudos e Projetos (Finep), Fundação de Amparo à Pesquisa do Estado de São Paulo (FAPESP) and The Sao Paulo Research Foundation (FAPESP), Brazil; Bulgarian Ministry of Education and Science, within the National Roadmap for Research Infrastructures 2020-2027 (object CERN), Bulgaria; Ministry of Education of China (MOEC), Ministry of Science & Technology of China (MSTC) and National Natural Science Foundation of China (NSFC), China; Ministry of Science and Education and Croatian Science Foundation, Croatia; Centro de Aplicaciones Tecnológicas y Desarrollo Nuclear (CEADEN), Cubaenergía, Cuba; Ministry of Education, Youth and Sports of the Czech Republic, Czech Republic; The Danish Council for Independent Research | Natural Sciences, the VILLUM FONDEN and Danish National Research Foundation (DNRF), Denmark; Helsinki Institute of Physics (HIP), Finland; Commissariat à l’Energie Atomique (CEA) and Institut National de Physique Nucléaire et de Physique des Particules (IN2P3) and Centre National de la Recherche Scientifique (CNRS), France; Bundesministerium für Forschung, Technologie und Raumfahrt (BMFTR) and GSI Helmholtzzentrum für Schwerionenforschung GmbH, Germany; National Research, Development and Innovation Office, Hungary; Department of Atomic Energy Government of India (DAE), Department of Science and Technology, Government of India (DST), University Grants Commission, Government of India (UGC) and Council of Scientific and Industrial Research (CSIR), India; National Research and Innovation Agency - BRIN, Indonesia; Istituto Nazionale di Fisica Nucleare (INFN), Italy; Japanese Ministry of Education, Culture, Sports, Science and Technology (MEXT) and Japan Society for the Promotion of Science (JSPS) KAKENHI, Japan; Consejo Nacional de Ciencia (CONACYT) y Tecnología, through Fondo de Cooperación Internacional en Ciencia y Tecnología (FONCICYT) and Dirección General de Asuntos del Personal Académico (DGAPA), Mexico; Nederlandse Organisatie voor Wetenschappelijk Onderzoek (NWO), Netherlands; The Research Council of Norway, Norway; Pontificia Universidad Católica del Perú, Peru; Ministry of Science and Higher Education, National Science Centre and WUT ID-UB, Poland; Korea Institute of Science and Technology Information and National Research Foundation of Korea (NRF), Republic of Korea; Ministry of Education and Scientific Research, Institute of Atomic Physics, Ministry of Research and Innovation and Institute of Atomic Physics and Universitatea Nationala de Stiinta si Tehnologie Politehnica Bucuresti, Romania; Ministerstvo školstva, vyzkumu, vyvoja a mladeze SR, Slovakia; National Research Foundation of South Africa, South Africa; Swedish Research Council (VR) and Knut & Alice Wallenberg Foundation (KAW), Sweden; European Organization for Nuclear Research, Switzerland; Suranaree University of Technology (SUT), National Science and Technology Development Agency (NSTDA) and National Science, Research and Innovation Fund (NSRF via PMU-B B05F650021), Thailand; Turkish Energy, Nuclear and Mineral Research Agency (TENMAK), Turkey; National Academy of Sciences of Ukraine, Ukraine; Science and Technology Facilities Council (STFC), United Kingdom; National Science Foundation of the United States of America (NSF) and United States Department of Energy, Office of Nuclear Physics (DOE NP), United States of America. In addition, individual groups or members have received support from: FORTE project, reg. no.

CZ.02.01.01/00/22_008/0004632, Czech Republic, co-funded by the European Union, Czech Republic; European Research Council (grant no. 950692), European Union; Deutsche Forschungs Gemeinschaft (DFG, German Research Foundation) “Neutrinos and Dark Matter in Astro- and Particle Physics” (grant no. SFB 1258), Germany; FAIR - Future Artificial Intelligence Research, funded by the NextGenerationEU program (Italy).

References

- [1] N. Brambilla *et al.*, “Heavy Quarkonium: Progress, Puzzles, and Opportunities”, *Eur. Phys. J. C* **71** (2011) 1534, arXiv:1010.5827 [hep-ph].
- [2] ALICE Collaboration, S. Acharya *et al.*, “The ALICE experiment: a journey through QCD”, *Eur. Phys. J. C* **84** (2024) 813, arXiv:2211.04384 [nucl-ex].
- [3] J. F. Amundson, O. J. P. Eboli, E. M. Gregores, and F. Halzen, “Quantitative tests of color evaporation: Charmonium production”, *Phys. Lett. B* **390** (1997) 323–328, arXiv:hep-ph/9605295.
- [4] H. Fritzsche, “Producing Heavy Quark Flavors in Hadronic Collisions: A Test of Quantum Chromodynamics”, *Phys. Lett. B* **67** (1977) 217–221.
- [5] J.-P. Lansberg, H.-S. Shao, N. Yamanaka, Y.-J. Zhang, and C. Noûs, “Complete NLO QCD study of single- and double-quarkonium hadroproduction in the colour-evaporation model at the Tevatron and the LHC”, *Phys. Lett. B* **807** (2020) 135559, arXiv:2004.14345 [hep-ph].
- [6] J. P. Lansberg, “ J/ψ production at $\sqrt{s} = 1.96$ and 7 TeV: Color-Singlet Model, NNLO* and polarisation”, *J. Phys. G* **38** (2011) 124110, arXiv:1107.0292 [hep-ph].
- [7] M. Butenschoen and B. A. Kniehl, “Next-to-leading-order tests of NRQCD factorization with J/ψ yield and polarization”, *Mod. Phys. Lett. A* **28** (2013) 1350027, arXiv:1212.2037 [hep-ph].
- [8] K.-T. Chao, Y.-Q. Ma, H.-S. Shao, K. Wang, and Y.-J. Zhang, “ J/ψ Polarization at Hadron Colliders in Nonrelativistic QCD”, *Phys. Rev. Lett.* **108** (2012) 242004, arXiv:1201.2675 [hep-ph].
- [9] Y.-Q. Ma, K. Wang, and K.-T. Chao, “A complete NLO calculation of the J/ψ and ψ' production at hadron colliders”, *Phys. Rev. D* **84** (2011) 114001, arXiv:1012.1030 [hep-ph].
- [10] LHCb Collaboration, R. Aaij *et al.*, “Measurement of J/ψ production in pp collisions at $\sqrt{s} = 2.76$ TeV”, *JHEP* **02** (2013) 041, arXiv:1212.1045 [hep-ex].
- [11] ALICE Collaboration, B. Abelev *et al.*, “Inclusive J/ψ production in pp collisions at $\sqrt{s} = 2.76$ TeV”, *Phys. Lett. B* **718** (2012) 295–306, arXiv:1203.3641 [hep-ex]. [Erratum: Phys.Lett.B 748, 472–473 (2015)].
- [12] ALICE Collaboration, S. Acharya *et al.*, “Inclusive J/ψ production at mid-rapidity in pp collisions at $\sqrt{s} = 5.02$ TeV”, *JHEP* **10** (2019) 084, arXiv:1905.07211 [nucl-ex].
- [13] ALICE Collaboration, J. Adam *et al.*, “ J/ψ suppression at forward rapidity in Pb–Pb collisions at $\sqrt{s_{NN}} = 5.02$ TeV”, *Phys. Lett. B* **766** (2017) 212–224, arXiv:1606.08197 [nucl-ex].
- [14] ALICE Collaboration, S. Acharya *et al.*, “Energy dependence of forward-rapidity J/ψ and $\psi(2S)$ production in pp collisions at the LHC”, *Eur. Phys. J. C* **77** (2017) 392, arXiv:1702.00557 [hep-ex].

- [15] **ATLAS** Collaboration, M. Aaboud *et al.*, “Measurement of quarkonium production in proton–lead and proton–proton collisions at 5.02 TeV with the ATLAS detector”, *Eur. Phys. J. C* **78** (2018) 171, arXiv:1709.03089 [nucl-ex].
- [16] **CMS** Collaboration, A. M. Sirunyan *et al.*, “Measurement of prompt and nonprompt J/ψ production in pp and pPb collisions at $\sqrt{s_{NN}} = 5.02$ TeV”, *Eur. Phys. J. C* **77** (2017) 269, arXiv:1702.01462 [nucl-ex].
- [17] **CMS** Collaboration, A. M. Sirunyan *et al.*, “Measurement of prompt and nonprompt charmonium suppression in PbPb collisions at 5.02 TeV”, *Eur. Phys. J. C* **78** (2018) 509, arXiv:1712.08959 [nucl-ex]. [Erratum: *Eur.Phys.J.C* 83, 145 (2023)].
- [18] **ALICE** Collaboration, S. Acharya *et al.*, “Prompt and non-prompt J/ψ production cross sections at midrapidity in proton–proton collisions at $\sqrt{s} = 5.02$ and 13 TeV”, *JHEP* **03** (2022) 190, arXiv:2108.02523 [nucl-ex].
- [19] **ALICE** Collaboration, S. Acharya *et al.*, “Inclusive quarkonium production in pp collisions at $\sqrt{s} = 5.02$ TeV”, *Eur. Phys. J. C* **83** (2023) 61, arXiv:2109.15240 [nucl-ex].
- [20] **LHCb** Collaboration, R. Aaij *et al.*, “Measurement of J/ψ production cross-sections in pp collisions at $\sqrt{s} = 5$ TeV”, *JHEP* **11** (2021) 181, arXiv:2109.00220 [hep-ex].
- [21] **ALICE** Collaboration, B. Abelev *et al.*, “Measurement of prompt J/ψ and beauty hadron production cross sections at mid-rapidity in pp collisions at $\sqrt{s} = 7$ TeV”, *JHEP* **11** (2012) 065, arXiv:1205.5880 [hep-ex].
- [22] **ALICE** Collaboration, B. Abelev *et al.*, “Measurement of quarkonium production at forward rapidity in pp collisions at $\sqrt{s} = 7$ TeV”, *Eur. Phys. J. C* **74** (2014) 2974, arXiv:1403.3648 [nucl-ex].
- [23] **LHCb** Collaboration, R. Aaij *et al.*, “Measurement of J/ψ production in pp collisions at $\sqrt{s} = 7$ TeV”, *Eur. Phys. J. C* **71** (2011) 1645, arXiv:1103.0423 [hep-ex].
- [24] **CMS** Collaboration, V. Khachatryan *et al.*, “Prompt and Non-Prompt J/ψ Production in pp Collisions at $\sqrt{s} = 7$ TeV”, *Eur. Phys. J. C* **71** (2011) 1575, arXiv:1011.4193 [hep-ex].
- [25] **ATLAS** Collaboration, G. Aad *et al.*, “Measurement of the differential cross-sections of inclusive, prompt and non-prompt J/ψ production in proton-proton collisions at $\sqrt{s} = 7$ TeV”, *Nucl. Phys. B* **850** (2011) 387–444, arXiv:1104.3038 [hep-ex].
- [26] **CMS** Collaboration, V. Khachatryan *et al.*, “Measurement of J/ψ and $\psi(2S)$ Prompt Double-Differential Cross Sections in pp Collisions at $\sqrt{s} = 7$ TeV”, *Phys. Rev. Lett.* **114** (2015) 191802, arXiv:1502.04155 [hep-ex].
- [27] **ALICE** Collaboration, J. Adam *et al.*, “Inclusive quarkonium production at forward rapidity in pp collisions at $\sqrt{s} = 8$ TeV”, *Eur. Phys. J. C* **76** (2016) 184, arXiv:1509.08258 [hep-ex].
- [28] **LHCb** Collaboration, R. Aaij *et al.*, “Production of J/ψ and Upsilon mesons in pp collisions at $\sqrt{s} = 8$ TeV”, *JHEP* **06** (2013) 064, arXiv:1304.6977 [hep-ex].
- [29] **ATLAS** Collaboration, G. Aad *et al.*, “Measurement of the differential cross-sections of prompt and non-prompt production of J/ψ and $\psi(2S)$ in pp collisions at $\sqrt{s} = 7$ and 8 TeV with the ATLAS detector”, *Eur. Phys. J. C* **76** (2016) 283, arXiv:1512.03657 [hep-ex].
- [30] **ALICE** Collaboration, S. Acharya *et al.*, “Inclusive J/ψ production at midrapidity in pp collisions at $\sqrt{s} = 13$ TeV”, *Eur. Phys. J. C* **81** (2021) 1121, arXiv:2108.01906 [nucl-ex].

- [31] **LHCb** Collaboration, R. Aaij *et al.*, “Measurement of forward J/ψ production cross-sections in pp collisions at $\sqrt{s} = 13$ TeV”, *JHEP* **10** (2015) 172, arXiv:1509.00771 [hep-ex]. [Erratum: *JHEP* **05**, 063 (2017)].
- [32] **CMS** Collaboration, A. M. Sirunyan *et al.*, “Measurement of quarkonium production cross sections in pp collisions at $\sqrt{s} = 13$ TeV”, *Phys. Lett. B* **780** (2018) 251–272, arXiv:1710.11002 [hep-ex].
- [33] **ATLAS** Collaboration, G. Aad *et al.*, “Measurement of the production cross-section of J/ψ and $\psi(2S)$ mesons in pp collisions at $\sqrt{s} = 13$ TeV with the ATLAS detector”, *Eur. Phys. J. C* **84** (2024) 169, arXiv:2309.17177 [hep-ex].
- [34] **ALICE** Collaboration, B. Abelev *et al.*, “ J/ψ polarization in pp collisions at $\sqrt{s} = 7$ TeV”, *Phys. Rev. Lett.* **108** (2012) 082001, arXiv:1111.1630 [hep-ex].
- [35] **CMS** Collaboration, S. Chatrchyan *et al.*, “Measurement of the Prompt J/ψ and $\psi(2S)$ Polarizations in pp Collisions at $\sqrt{s} = 7$ TeV”, *Phys. Lett. B* **727** (2013) 381–402, arXiv:1307.6070 [hep-ex].
- [36] **LHCb** Collaboration, R. Aaij *et al.*, “Measurement of J/ψ polarization in pp collisions at $\sqrt{s} = 7$ TeV”, *Eur. Phys. J. C* **73** (2013) 2631, arXiv:1307.6379 [hep-ex].
- [37] **ALICE** Collaboration, S. Acharya *et al.*, “Measurement of the inclusive J/ψ polarization at forward rapidity in pp collisions at $\sqrt{s} = 8$ TeV”, *Eur. Phys. J. C* **78** (2018) 562, arXiv:1805.04374 [hep-ex].
- [38] **ALICE** Collaboration, S. Acharya *et al.*, “ J/ψ -hadron correlations at midrapidity in pp collisions at $\sqrt{s} = 13$ TeV”, *JHEP* **07** (2025) 023, arXiv:2409.04364 [nucl-ex].
- [39] Y.-Q. Ma and R. Vogt, “Quarkonium Production in an Improved Color Evaporation Model”, *Phys. Rev. D* **94** (2016) 114029, arXiv:1609.06042 [hep-ph].
- [40] V. Cheung and R. Vogt, “Production and polarization of prompt J/ψ in the improved color evaporation model using the k_T -factorization approach”, *Phys. Rev. D* **98** (2018) 114029, arXiv:1808.02909 [hep-ph].
- [41] M. Butenschoen and B. A. Kniehl, “ J/ψ polarization at Tevatron and LHC: Nonrelativistic-QCD factorization at the crossroads”, *Phys. Rev. Lett.* **108** (2012) 172002, arXiv:1201.1872 [hep-ph].
- [42] B. Gong, L.-P. Wan, J.-X. Wang, and H.-F. Zhang, “Polarization for Prompt J/ψ and $\psi(2s)$ Production at the Tevatron and LHC”, *Phys. Rev. Lett.* **110** (2013) 042002, arXiv:1205.6682 [hep-ph].
- [43] M. Butenschoen and B. A. Kniehl, “World data of J/ψ production consolidate NRQCD factorization at NLO”, *Phys. Rev. D* **84** (2011) 051501, arXiv:1105.0820 [hep-ph].
- [44] G. T. Bodwin, H. S. Chung, U.-R. Kim, and J. Lee, “Fragmentation contributions to J/ψ production at the Tevatron and the LHC”, *Phys. Rev. Lett.* **113** (2014) 022001, arXiv:1403.3612 [hep-ph].
- [45] P. Faccioli, V. Knünz, C. Lourenco, J. Seixas, and H. K. Wöhri, “Quarkonium production in the LHC era: a polarized perspective”, *Phys. Lett. B* **736** (2014) 98–109, arXiv:1403.3970 [hep-ph].

- [46] G. T. Bodwin, K.-T. Chao, H. S. Chung, U.-R. Kim, J. Lee, and Y.-Q. Ma, “Fragmentation contributions to hadroproduction of prompt J/ψ , χ_{cJ} , and $\psi(2S)$ states”, *Phys. Rev. D* **93** (2016) 034041, arXiv:1509.07904 [hep-ph].
- [47] P. Faccioli, C. Lourenço, M. Araújo, V. Knünz, I. Krätschmer, and J. Seixas, “Quarkonium production at the LHC: A data-driven analysis of remarkably simple experimental patterns”, *Phys. Lett. B* **773** (2017) 476–486, arXiv:1702.04208 [hep-ph].
- [48] P. Faccioli, C. Lourenço, M. Araújo, J. Seixas, I. Krätschmer, and V. Knünz, “From identical S- and P-wave p_T spectra to maximally distinct polarizations: probing NRQCD with χ states”, *Eur. Phys. J. C* **78** (2018) 268, arXiv:1802.01106 [hep-ph].
- [49] M. Baumgart, A. K. Leibovich, T. Mehen, and I. Z. Rothstein, “Probing Quarkonium Production Mechanisms with Jet Substructure”, *JHEP* **11** (2014) 003, arXiv:1406.2295 [hep-ph].
- [50] **LHCb** Collaboration, R. Aaij *et al.*, “Study of J/ψ Production in Jets”, *Phys. Rev. Lett.* **118** (2017) 192001, arXiv:1701.05116 [hep-ex].
- [51] **CMS** Collaboration, A. Tumasyan *et al.*, “Fragmentation of jets containing a prompt J/ψ meson in PbPb and pp collisions at $\sqrt{s_{NN}} = 5.02$ TeV”, *Phys. Lett. B* **825** (2022) 136842, arXiv:2106.13235 [hep-ex].
- [52] **LHCb** Collaboration, R. Aaij *et al.*, “Measurements of $\psi(2S)$ and $\chi_{c1}(3872)$ production within fully reconstructed jets”, *Eur. Phys. J. C* **85** (2025) 562, arXiv:2410.18018 [hep-ex].
- [53] R. Bain, Y. Makris, and T. Mehen, “Transverse Momentum Dependent Fragmenting Jet Functions with Applications to Quarkonium Production”, *JHEP* **11** (2016) 144, arXiv:1610.06508 [hep-ph].
- [54] R. Bain, L. Dai, A. Leibovich, Y. Makris, and T. Mehen, “NRQCD Confronts LHCb Data on Quarkonium Production within Jets”, *Phys. Rev. Lett.* **119** (2017) 032002, arXiv:1702.05525 [hep-ph].
- [55] N. Cooke, P. Ilten, L. Lönnblad, and S. Mrenna, “Non-relativistic quantum chromodynamics in parton showers”, *Eur. Phys. J. C* **84** (2024) 432, arXiv:2312.05203 [hep-ph].
- [56] J. C. Collins, D. E. Soper, and G. F. Sterman, “Factorization for Short Distance Hadron - Hadron Scattering”, *Nucl. Phys. B* **261** (1985) 104–142.
- [57] **ALICE** Collaboration, S. Acharya *et al.*, “Charm-quark fragmentation fractions and production cross section at midrapidity in pp collisions at the LHC”, *Phys. Rev. D* **105** (2022) L011103, arXiv:2105.06335 [nucl-ex].
- [58] **ALICE** Collaboration, S. Acharya *et al.*, “Measurement of the fraction of jet longitudinal momentum carried by Λ_c^+ baryons in pp collisions”, *Phys. Rev. D* **109** (2024) 072005, arXiv:2301.13798 [nucl-ex].
- [59] A. Bazavov *et al.*, “Equation of state and QCD transition at finite temperature”, *Phys. Rev. D* **80** (2009) 014504, arXiv:0903.4379 [hep-lat].
- [60] S. Borsanyi, Z. Fodor, C. Hoelbling, S. D. Katz, S. Krieg, and K. K. Szabo, “Full result for the QCD equation of state with 2+1 flavors”, *Phys. Lett. B* **730** (2014) 99–104, arXiv:1309.5258 [hep-lat].
- [61] T. Matsui and H. Satz, “ J/ψ Suppression by Quark-Gluon Plasma Formation”, *Phys. Lett. B* **178** (1986) 416–422.

- [62] R. L. Thews, M. Schroedter, and J. Rafelski, “Enhanced J/ψ production in deconfined quark matter”, *Phys. Rev. C* **63** (2001) 054905, arXiv:hep-ph/0007323.
- [63] P. Braun-Munzinger and J. Stachel, “(Non)thermal aspects of charmonium production and a new look at J/ψ suppression”, *Phys. Lett. B* **490** (2000) 196–202, arXiv:nucl-th/0007059.
- [64] J. D. Bjorken, “Energy loss of energetic partons in quark-gluon plasma”, tech. rep., FERMILAB, Batavia, IL, 1982. <https://cds.cern.ch/record/141477>.
- [65] A. Andronic, P. Braun-Munzinger, M. K. Köhler, K. Redlich, and J. Stachel, “Transverse momentum distributions of charmonium states with the statistical hadronization model”, *Phys. Lett. B* **797** (2019) 134836, arXiv:1901.09200 [nucl-th].
- [66] X. Zhao and R. Rapp, “Transverse Momentum Spectra of J/ψ in Heavy-Ion Collisions”, *Phys. Lett. B* **664** (2008) 253–257, arXiv:0712.2407 [hep-ph].
- [67] K. Zhou, N. Xu, Z. Xu, and P. Zhuang, “Medium effects on charmonium production at ultrarelativistic energies available at the CERN Large Hadron Collider”, *Phys. Rev. C* **89** (2014) 054911, arXiv:1401.5845 [nucl-th].
- [68] ALICE Collaboration, S. Acharya *et al.*, “Measurements of inclusive J/ψ production at midrapidity and forward rapidity in Pb–Pb collisions at $\sqrt{s_{NN}} = 5.02$ TeV”, *Phys. Lett. B* **849** (2024) 138451, arXiv:2303.13361 [nucl-ex].
- [69] ALICE Collaboration, S. Acharya *et al.*, “ J/ψ elliptic and triangular flow in Pb–Pb collisions at $\sqrt{s_{NN}} = 5.02$ TeV”, *JHEP* **10** (2020) 141, arXiv:2005.14518 [nucl-ex].
- [70] M. He, B. Wu, and R. Rapp, “Collectivity of J/ψ Mesons in Heavy-Ion Collisions”, *Phys. Rev. Lett.* **128** (2022) 162301, arXiv:2111.13528 [nucl-th].
- [71] P. Caucal, E. Iancu, A. H. Mueller, and G. Soyez, “Vacuum-like jet fragmentation in a dense QCD medium”, *Phys. Rev. Lett.* **120** (2018) 232001, arXiv:1801.09703 [hep-ph].
- [72] H. S. Chung, “Review of quarkonium production: status and prospects”, *PoS Confinement2018* (2018) 007, arXiv:1811.12098 [hep-ph].
- [73] M. Cacciari, G. P. Salam, and G. Soyez, “The anti- k_t jet clustering algorithm”, *JHEP* **04** (2008) 063, arXiv:0802.1189 [hep-ph].
- [74] ALICE Collaboration, K. Aamodt *et al.*, “The ALICE experiment at the CERN LHC”, *JINST* **3** (2008) S08002.
- [75] ALICE Collaboration, B. Abelev *et al.*, “Performance of the ALICE Experiment at the CERN LHC”, *Int. J. Mod. Phys. A* **29** (2014) 1430044, arXiv:1402.4476 [nucl-ex].
- [76] ALICE Collaboration, G. Dellacasa *et al.*, “ALICE: Technical design report of the time projection chamber”, CERN-OPEN-2000-183, CERN-LHCC-2000-001.
- [77] ALICE Collaboration, S. Acharya *et al.*, “The ALICE Transition Radiation Detector: construction, operation, and performance”, *Nucl. Instrum. Meth. A* **881** (2018) 88–127, arXiv:1709.02743 [physics.ins-det].
- [78] ALICE Collaboration, E. Abbas *et al.*, “Performance of the ALICE VZERO system”, *JINST* **8** (2013) P10016, arXiv:1306.3130 [nucl-ex].
- [79] ALICE Collaboration, S. Acharya *et al.*, “ J/ψ production at midrapidity in p–Pb collisions at $\sqrt{s_{NN}} = 8.16$ TeV”, *JHEP* **07** (2023) 137, arXiv:2211.14153 [nucl-ex].

- [80] T. Sjostrand, S. Mrenna, and P. Z. Skands, “PYTHIA 6.4 Physics and Manual”, *JHEP* **05** (2006) 026, arXiv:hep-ph/0603175.
- [81] F. Bossu, Z. Conesa del Valle, A. de Falco, M. Gagliardi, S. Grigoryan, and G. Martinez Garcia, “Phenomenological interpolation of the inclusive J/ψ cross section to proton-proton collisions at 2.76 TeV and 5.5 TeV”, arXiv:1103.2394 [nucl-ex].
- [82] D. J. Lange, “The EvtGen particle decay simulation package”, *Nucl. Instrum. Meth. A* **462** (2001) 152–155.
- [83] E. Barberio and Z. Was, “PHOTOS: A Universal Monte Carlo for QED radiative corrections. Version 2.0”, *Comput. Phys. Commun.* **79** (1994) 291–308.
- [84] R. Brun, F. Bruyant, F. Carminati, S. Giani, M. Maire, A. McPherson, G. Patrick, and L. Urban, *GEANT: Detector Description and Simulation Tool; Oct 1994*. CERN Program Library. CERN, Geneva, 1993. <https://cds.cern.ch/record/1082634>.
- [85] M. Cacciari, G. P. Salam, and G. Soyez, “FastJet User Manual”, *Eur. Phys. J. C* **72** (2012) 1896, arXiv:1111.6097 [hep-ph].
- [86] **Particle Data Group** Collaboration, R. L. Workman *et al.*, “Review of Particle Physics”, *PTEP* **2022** (2022) 083C01.
- [87] **ALICE** Collaboration, J. Adam *et al.*, “Inclusive, prompt and non-prompt J/ψ production at mid-rapidity in Pb–Pb collisions at $\sqrt{s_{NN}} = 2.76$ TeV”, *JHEP* **07** (2015) 051, arXiv:1504.07151 [nucl-ex].
- [88] G. D’Agostini, “A multidimensional unfolding method based on Bayes’ theorem”, *Nucl. Instrum. Meth. A* **362** (1995) 487–498.
- [89] T. Auye, “RooUnfold, a framework for unfolding within the ROOT environment.” January, 2021. <https://gitlab.cern.ch/RooUnfold/RooUnfold>.
- [90] **ALICE** Collaboration, S. Acharya *et al.*, “Measurements of inclusive jet spectra in pp and central Pb–Pb collisions at $\sqrt{s_{NN}} = 5.02$ TeV”, *Phys. Rev. C* **101** (2020) 034911, arXiv:1909.09718 [nucl-ex].
- [91] **ALICE** Collaboration, S. Acharya *et al.*, “Measurement of the production of charm jets tagged with D^0 mesons in pp collisions at $\sqrt{s} = 5.02$ and 13 TeV”, *JHEP* **06** (2023) 133, arXiv:2204.10167 [nucl-ex].
- [92] P. Skands, S. Carrazza, and J. Rojo, “Tuning PYTHIA 8.1: the Monash 2013 Tune”, *Eur. Phys. J. C* **74** (2014) 3024, arXiv:1404.5630 [hep-ph].
- [93] S.-L. Zhang and H. Xing, “ J/ψ production within a jet in high-energy proton-proton and nucleus-nucleus collisions”, *Phys. Lett. B* **863** (2025) 139382, arXiv:2403.12704 [hep-ph].
- [94] Z.-B. Kang, J.-W. Qiu, F. Ringer, H. Xing, and H. Zhang, “ J/ψ production and polarization within a jet”, *Phys. Rev. Lett.* **119** (2017) 032001, arXiv:1702.03287 [hep-ph].
- [95] J. Alwall, R. Frederix, S. Frixione, V. Hirschi, F. Maltoni, O. Mattelaer, H. S. Shao, T. Stelzer, P. Torrielli, and M. Zaro, “The automated computation of tree-level and next-to-leading order differential cross sections, and their matching to parton shower simulations”, *JHEP* **07** (2014) 079, arXiv:1405.0301 [hep-ph].
- [96] Y.-Q. Ma, J.-W. Qiu, and H. Zhang, “Heavy quarkonium fragmentation functions from a heavy quark pair. I. S wave”, *Phys. Rev. D* **89** (2014) 094029, arXiv:1311.7078 [hep-ph].

A The ALICE Collaboration

D.A.H. Abdallah¹³⁴, I.J. Abualrob¹¹², S. Acharya⁴⁹, G. Aglieri Rinella³², L. Aglietta²⁴, N. Agrawal²⁵, Z. Ahammed¹³², S. Ahmad¹⁵, I. Ahuja³⁶, Z. Akbar⁷⁹, V. Akishina³⁸, M. Al-Turany⁹⁴, B. Alessandro⁵⁵, R. Alfaro Molina⁶⁶, B. Ali¹⁵, A. Alici^{1,25}, J. Alme²⁰, G. Alocco²⁴, T. Alt⁶³, I. Altsybeev⁹², C. Andrei⁴⁴, N. Andreou¹¹¹, A. Andronic¹²³, M. Angeletti³², V. Anguelov⁹¹, F. Antinori⁵³, P. Antonioli⁵⁰, N. Apadula⁷¹, H. Appelshäuser⁶³, S. Arcelli^{1,25}, R. Arnaldi⁵⁵, I.C. Arsene¹⁹, M. Arslandok¹³⁵, A. Augustinus³², R. Averbeck⁹⁴, M.D. Azmi¹⁵, H. Baba¹²¹, A.R.J. Babu¹³⁴, A. Badalà⁵², J. Bae¹⁰⁰, Y. Bae¹⁰⁰, Y.W. Baek¹⁰⁰, X. Bai¹¹⁶, R. Bailhache⁶³, Y. Bailung^{125,47}, R. Bala⁸⁸, A. Baldisseri¹²⁷, B. Balis², S. Bangalia¹¹⁴, Z. Banoo⁸⁸, V. Barbasova³⁶, F. Barile³¹, L. Barioglio⁵⁵, M. Barlou²⁴, B. Barman⁴⁰, G.G. Barnaföldi⁴⁵, L.S. Barnby¹¹¹, E. Barreau⁹⁹, V. Barret¹²⁴, L. Barreto¹⁰⁶, K. Barth³², E. Bartsch⁶³, N. Bastid¹²⁴, G. Batigne⁹⁹, D. Battistini^{34,92}, B. Batyunya¹³⁹, L. Baudino²⁴, D. Bauri⁴⁶, J.L. Bazo Alba⁹⁸, I.G. Bearden⁸⁰, P. Becht⁹⁴, D. Behera^{77,47}, S. Behera⁴⁶, I. Belikov¹²⁶, V.D. Bella¹²⁶, F. Bellini²⁵, R. Bellwied¹¹², L.G.E. Beltran¹⁰⁵, Y.A.V. Beltran⁴³, G. Bencedi⁴⁵, O. Benchikhi⁷³, A. Bensaoula¹¹², S. Beole²⁴, A. Berdnikova⁹¹, L. Bergmann⁷¹, L. Bernardinis²³, L. Betev³², P.P. Bhaduri¹³², T. Bhalla⁸⁷, A. Bhasin⁸⁸, B. Bhattacharjee⁴⁰, L. Bianchi²⁴, J. Bielčik³⁴, J. Bielčíková⁸³, A. Bilandzic⁹², A. Binoy¹¹⁴, G. Biro⁴⁵, S. Biswas⁴, M.B. Blidaru⁹⁴, N. Bluhme³⁸, C. Blume⁶³, F. Bock⁸⁴, T. Bodova²⁰, L. Boldizsár⁴⁵, M. Bombara³⁶, P.M. Bond³², G. Bonomi^{131,54}, H. Borel¹²⁷, A. Borissov¹³⁹, A.G. Borquez Carcamo⁹¹, E. Botta²⁴, N. Bouchhar¹⁷, Y.E.M. Bouziani⁶³, D.C. Brandibur⁶², L. Bratrud⁶³, P. Braun-Munzinger⁹⁴, M. Bregant¹⁰⁶, M. Broz³⁴, G.E. Bruno^{93,31}, V.D. Buchakchiev³⁵, M.D. Buckland⁸², H. Buesching⁶³, S. Bufalino²⁹, P. Buhler⁷³, N. Burmasov¹³⁹, Z. Buthelezi^{67,120}, A. Bylinkin²⁰, C. Carr⁹⁷, J.C. Cabanillas Noris¹⁰⁵, M.F.T. Cabrera¹¹², H. Caines¹³⁵, A. Caliva²⁸, E. Calvo Villar⁹⁸, J.M.M. Camacho¹⁰⁵, P. Camerini²³, M.T. Camerlingo⁴⁹, F.D.M. Canedo¹⁰⁶, S. Cannito²³, S.L. Cantway¹³⁵, M. Carabas¹⁰⁹, F. Carnesecchi³², L.A.D. Carvalho¹⁰⁶, J. Castillo Castellanos¹²⁷, M. Castoldi³², F. Catalano³², S. Cattaruzzi²³, R. Cerri²⁴, I. Chakaberia⁷¹, P. Chakraborty¹³³, J.W.O. Chan¹¹², S. Chandra¹³², S. Chapeland³², M. Chartier¹¹⁵, S. Chattopadhyay¹³², M. Chen³⁹, T. Cheng⁶, C. Cheshkov¹²⁵, D. Chiappara²⁷, V. Chibante Barroso³², D.D. Chinellato⁷³, F. Chinu²⁴, E.S. Chizzali^{11,92}, J. Cho⁵⁷, S. Cho⁵⁷, P. Chochula³², Z.A. Chochulska^{111,133}, P. Christakoglou⁸¹, C.H. Christensen⁸⁰, P. Christiansen⁷², T. Chujo¹²², B. Chytla¹³³, M. Ciacco²⁴, C. Cicalo⁵¹, G. Cimdor^{32,24}, F. Cindolo⁵⁰, F. Colamaria⁴⁹, D. Colella³¹, A. Colelli³¹, M. Colocci²⁵, M. Concas³², G. Conesa Balbastre⁷⁰, Z. Conesa del Valle¹²⁸, G. Contin²³, J.G. Contreras³⁴, M.L. Coquet⁹⁹, P. Cortese^{130,55}, M.R. Cosentino¹⁰⁸, F. Costa³², S. Costanza²¹, P. Crochet¹²⁴, M.M. Czarnynoga¹³³, A. Dainese⁵³, E. Dall'occo³², G. Dange³⁸, M.C. Danisch¹⁶, A. Danu⁶², A. Daribayeva³⁸, P. Das³², S. Das⁴, A.R. Dash¹²³, S. Dash⁴⁶, A. De Caro²⁸, G. de Cataldo⁴⁹, J. de Cuveland³⁸, A. De Falco²², D. De Gruttola²⁸, N. De Marco⁵⁵, C. De Martin²³, S. De Pasquale²⁸, R. Deb¹³¹, R. Del Grande³⁴, L. Dello Stritto³², G.G.A. de Souza^{14,106}, P. Dhankeer¹⁸, D. Di Bari³¹, M. Di Costanzo²⁹, A. Di Mauro³², B. Di Ruzza^{1,129,49}, B. Diab³², Y. Ding⁶, J. Ditzel⁶³, R. Divià³², U. Dmitrieva⁵⁵, A. Dobrin⁶², B. Dönigus⁶³, L. Döpfer⁴¹, J.M. Dubinski¹³³, A. Dubla⁹⁴, P. Dupieux¹²⁴, N. Dzalaiova¹³, T.M. Eder¹²³, R.J. Ehlers⁷¹, F. Eisenhut⁶³, R. Ejima⁸⁹, D. Elia⁴⁹, B. Erasmus⁹⁹, F. Ercolessi²⁵, B. Espagnon¹²⁸, G. Eulisse³², D. Evans⁹⁷, L. Fabbietti⁹², G. Fabbri⁵⁰, M. Faggin³², J. Faivre⁷⁰, W. Fan¹¹², T. Fang⁶, A. Fantoni⁴⁸, A. Feliciello⁵⁵, W. Feng⁶, A. Fernández Téllez⁴³, B. Fernando¹³⁴, L. Ferrandi¹⁰⁶, A. Ferrero¹²⁷, C. Ferrero^{V,55}, A. Ferretti²⁴, D. Finogeev¹³⁹, F.M. Fionda⁵¹, A.N. Flores¹⁰⁴, S. Foertsch⁶⁷, I. Fokin⁹¹, U. Follo^{V,55}, R. Forynski¹¹¹, E. Fragiaco⁵⁶, H. Fribert⁹², U. Fuchs³², D. Fuligno²³, N. Funicello²⁸, C. Furget⁷⁰, A. Furs¹³⁹, T. Fusayasu⁹⁵, J.J. Gaardhøje⁸⁰, M. Gagliardi²⁴, A.M. Gago⁹⁸, T. Gahlaut⁴⁶, C.D. Galvan¹⁰⁵, S. Gami⁷⁷, C. Garabatos⁹⁴, J.M. Garcia⁴³, E. Garcia-Solis⁹, S. Garetti¹²⁸, C. Gargiulo³², P. Gasik⁹⁴, A. Gautam¹¹⁴, M.B. Gay Ducati⁶⁵, M. Germain⁹⁹, R.A. Gernhaeuser⁹², M. Giacalone³², G. Gioachin²⁹, S.K. Giri¹³², P. Giubellino⁵⁵, P. Giubilato²⁷, P. Glässel⁹¹, E. Glimos¹¹⁹, L. Gonella²³, V. Gonzalez¹³⁴, M. Gorgon², K. Goswami⁴⁷, S. Gotovac³³, V. Grabski⁶⁶, L.K. Graczykowski¹³³, E. Grecka⁸³, A. Grelli⁵⁸, C. Grigoras³², S. Grigoryan^{139,1}, O.S. Groettvik³², M. Gronbeck⁴¹, F. Grosa³², S. Gross-Börling⁹⁴, J.F. Grosse-Oetringhaus³², R. Grosso⁹⁴, D. Grund³⁴, N.A. Grunwald⁹¹, R. Guernane⁷⁰, M. Guilbaud⁹⁹, K. Gulbrandsen⁸⁰, J.K. Gumprecht⁷³, T. Gündem⁶³, T. Gunji¹²¹, J. Guo¹⁰, W. Guo⁶, A. Gupta⁸⁸, R. Gupta⁸⁸, R. Gupta⁴⁷, K. Gwizdziel¹³³, L. Gyulai⁴⁵, T. Hachiya⁷⁵, C. Hadjidakis¹²⁸, F.U. Haider⁸⁸,

S. Haidlova³⁴, M. Haldar⁴, W. Ham¹⁰⁰, H. Hamagaki⁷⁴, Y. Han¹³⁷, R. Hannigan¹⁰⁴, J. Hansen⁷², J.W. Harris¹³⁵, A. Harton⁹, M.V. Hartung⁶³, A. Hasan¹¹⁸, H. Hassan¹¹³, D. Hatzifotiadiou⁵⁰, P. Hauer⁴¹, L.B. Havener¹³⁵, E. Hellbär³², H. Helstrup³⁷, M. Hemmer⁶³, S.G. Hernandez¹¹², G. Herrera Corral⁸, K.F. Hetland³⁷, B. Heybeck⁶³, H. Hillemanns³², B. Hippolyte¹²⁶, I.P.M. Hobus⁸¹, F.W. Hoffmann³⁸, B. Hofman⁵⁸, Y. Hong⁵⁷, A. Horzyk², Y. Hou^{94,11}, P. Hristov³², L.M. Huhta¹¹³, T.J. Humanic⁸⁵, V. Humlova³⁴, M. Husar⁸⁶, A. Hutson¹¹², D. Hutter³⁸, M.C. Hwang¹⁸, M. Inaba¹²², A. Isakov⁸¹, T. Isidori¹¹⁴, M.S. Islam⁴⁶, M. Ivanov⁹⁴, M. Ivanov¹³, K.E. Iversen⁷², J.G. Kim¹³⁷, M. Jablonski², B. Jacak^{18,71}, N. Jacazio²⁵, P.M. Jacobs⁷¹, A. Jadlovska¹⁰², S. Jadlovska¹⁰², S. Jaelani⁷⁹, C. Jahnke¹⁰⁷, M.J. Jakubowska¹³³, E.P. Jamro², D.M. Janik³⁴, M.A. Janik¹³³, S. Ji¹⁶, Y. Ji⁹⁴, S. Jia⁸⁰, T. Jiang¹⁰, A.A.P. Jimenez⁶⁴, S. Jin¹⁰, F. Jonas⁷¹, D.M. Jones¹¹⁵, J.M. Jowett^{32,94}, J. Jung⁶³, M. Jung⁶³, A. Junique³², J. Juracka³⁴, J. Kaewjai^{115,101}, P. Kalinak⁵⁹, A. Kalweit³², A. Karasu Uysal¹³⁶, N. Karatzenis⁹⁷, T. Karavicheva¹³⁹, M.J. Karwowska¹³³, V. Kashyap⁷⁷, M. Keil³², B. Ketzer⁴¹, J. Keul⁶³, S.S. Khade⁴⁷, A.M. Khan¹¹⁶, A. Khuntia⁵⁰, Z. Khuranova⁶³, B. Kileng³⁷, B. Kim¹⁰⁰, D.J. Kim¹¹³, D. Kim¹⁰⁰, E.J. Kim⁶⁸, G. Kim⁵⁷, H. Kim⁵⁷, J. Kim¹³⁷, J. Kim⁵⁷, J. Kim³², M. Kim¹⁸, S. Kim¹⁷, T. Kim¹³⁷, J.T. Kinner¹²³, I. Kisel³⁸, A. Kisiel¹³³, J.L. Klay⁵, J. Klein³², S. Klein⁷¹, C. Klein-Bösing¹²³, M. Kleiner⁶³, A. Kluge³², M.B. Knuesel¹³⁵, C. Kobdaj¹⁰¹, R. Kohara¹²¹, A. Kondratyev¹³⁹, J. Konig⁶³, P.J. Konopka³², G. Kornakov¹³³, M. Korwieser⁹², C. Koster⁸¹, A. Kotliarov⁸³, N. Kovacic⁸⁶, M. Kowalski¹⁰³, V. Kozhuharov³⁵, G. Kozlov³⁸, I. Králik⁵⁹, A. Kravčáková³⁶, M.A. Krawczyk³², L. Krcal³², F. Krizek⁸³, K. Krizkova Gajdosova³⁴, C. Krug⁶⁵, M. Krüger⁶³, E. Kryshen¹³⁹, V. Kučera⁵⁷, C. Kuhn¹²⁶, D. Kumar¹³², L. Kumar⁸⁷, N. Kumar⁸⁷, S. Kumar⁴⁹, S. Kundu³², M. Kuo¹²², P. Kurashvili⁷⁶, S. Kurita⁸⁹, S. Kushpil⁸³, A. Kuznetsov¹³⁹, M.J. Kweon⁵⁷, Y. Kwon¹³⁷, S.L. La Pointe³⁸, P. La Rocca²⁶, A. Lakrathok¹⁰¹, S. Lambert⁹⁹, A.R. Landou⁷⁰, R. Langoy¹¹⁸, P. Larionov³², E. Laudi³², L. Lautner⁹², R.A.N. Laveaga¹⁰⁵, R. Lavicka⁷³, R. Lea^{131,54}, J.B. Lebert³⁸, H. Lee¹⁰⁰, S. Lee⁵⁷, I. Legrand⁴⁴, G. Legras¹²³, A.M. Lejeune³⁴, T.M. Lelek², I. León Monzón¹⁰⁵, M.M. Lesch⁹², P. Lévai⁴⁵, M. Li⁶, P. Li¹⁰, X. Li¹⁰, B.E. Liang-Gilman¹⁸, J. Lien¹¹⁸, R. Lietava⁹⁷, I. Likmeta¹¹², B. Lim⁵⁵, H. Lim¹⁶, S.H. Lim¹⁶, Y.N. Lima¹⁰⁶, S. Lin¹⁰, V. Lindenstruth³⁸, C. Lippmann⁹⁴, D. Liskova¹⁰², D.H. Liu⁶, J. Liu¹¹⁵, Y. Liu⁶, G.S.S. Liveraro¹⁰⁷, I.M. Lofnes²⁰, C. Loizides²⁰, S. Lokos¹⁰³, J. Lömker⁵⁸, X. Lopez¹²⁴, E. López Torres⁷, C. Lotteau¹²⁵, P. Lu¹¹⁶, W. Lu⁶, Z. Lu¹⁰, O. Lubyets⁹⁴, G.A. Lucia²⁹, F.V. Lugo⁶⁶, J. Luo³⁹, G. Luparello⁵⁶, J. M. Friedrich⁹², Y.G. Ma³⁹, V. Machacek⁸⁰, M. Mager³², M. Mahlein⁹², A. Maire¹²⁶, E. Majerz², M.V. Makariev³⁵, G. Malfattore⁵⁰, N.M. Malik⁸⁸, N. Malik¹⁵, D. Mallick¹²⁸, N. Mallick¹¹³, G. Mandaglio^{30,52}, S.K. Mandal⁷⁶, A. Manea⁶², R. Manhart⁹², A.K. Manna⁴⁷, F. Manso¹²⁴, G. Mantzaridis⁹², V. Manzari⁴⁹, Y. Mao⁶, R.W. Marcjan², G.V. Margagliotti²³, A. Margotti⁵⁰, A. Marín⁹⁴, C. Markert¹⁰⁴, P. Martinengo³², M.I. Martínez⁴³, M.P.P. Martins^{32,106}, S. Masciocchi⁹⁴, M. Masera²⁴, A. Masoni⁵¹, L. Massacrier¹²⁸, O. Massen⁵⁸, A. Mastroserio^{129,49}, L. Mattei^{24,124}, S. Mattiazzo²⁷, A. Matyja¹⁰³, J.L. Mayo¹⁰⁴, F. Mazzaschi³², M. Mazzilli³¹, Y. Melikyan⁴², M. Melo¹⁰⁶, A. Menchaca-Rocha⁶⁶, J.E.M. Mendez⁶⁴, E. Meninno⁷³, M.W. Menzel^{32,91}, M. Meres¹³, L. Micheletti⁵⁵, D. Mihai¹⁰⁹, D.L. Mihaylov⁹², A.U. Mikalsen²⁰, K. Mikhaylov¹³⁹, L. Millot⁷⁰, N. Minafra¹¹⁴, D. Miśkowiec⁹⁴, A. Modak⁵⁶, B. Mohanty⁷⁷, M. Mohisin Khan^{VI,15}, M.A. Molander⁴², M.M. Mondal⁷⁷, S. Monira¹³³, D.A. Moreira De Godoy¹²³, A. Morsch³², C. Moscatelli²³, T. Mrnjavac³², S. Mrozinski⁶³, V. Muccifora⁴⁸, S. Muhuri¹³², A. Mulliri²², M.G. Munhoz¹⁰⁶, R.H. Munzer⁶³, L. Musa³², J. Musinsky⁵⁹, J.W. Myrcha¹³³, B. Naik¹²⁰, A.I. Nambrath¹⁸, B.K. Nandi⁴⁶, R. Nania⁵⁰, E. Nappi⁴⁹, A.F. Nassirpour¹⁷, V. Nastase¹⁰⁹, A. Nath⁹¹, N.F. Nathanson⁸⁰, A. Neagu¹⁹, L. Nellen⁶⁴, R. Nepeivoda⁷², S. Nese¹⁹, N. Nicassio³¹, B.S. Nielsen⁸⁰, E.G. Nielsen⁸⁰, F. Noferini⁵⁰, S. Noh¹², P. Nomokonov¹³⁹, J. Norman¹¹⁵, N. Novitzky⁸⁴, J. Nystrand²⁰, M.R. Ockleton¹¹⁵, M. Ogino⁷⁴, J. Oh¹⁶, S. Oh¹⁷, A. Ohlson⁷², M. Oida⁸⁹, L.A.D. Oliveira^{I,107}, C. Oppedisano⁵⁵, A. Ortiz Velasquez⁶⁴, H. Osanai⁷⁴, J. Otwinowski¹⁰³, M. Oya⁸⁹, K. Oyama⁷⁴, S. Padhan^{131,46}, D. Pagano^{131,54}, G. Paić⁶⁴, A. Palasciano^{93,49}, I. Panasenkov⁷², P. Panigrahi⁴⁶, C. Pantouvakis²⁷, H. Park¹²², J. Park¹²², S. Park¹⁰⁰, T.Y. Park¹³⁷, J.E. Parkkila¹³³, P.B. Pati⁸⁰, Y. Patley⁴⁶, R.N. Patra⁴⁹, B. Paul¹³², F. Pazdic⁹⁷, H. Pei⁶, T. Peitzmann⁵⁸, X. Peng^{53,11}, S. Perciballi²⁴, G.M. Perez⁷, M. Petrovici⁴⁴, S. Piano⁵⁶, M. Pikna¹³, P. Pillot⁹⁹, O. Pinazza^{50,32}, C. Pinto³², S. Pisano⁴⁸, M. Płoskoń⁷¹, A. Plachta¹³³, M. Planinic⁸⁶, D.K. Plociennik², S. Politano³², N. Poljak⁸⁶, A. Pop⁴⁴, S. Porteboeuf-Houssais¹²⁴, J.S. Potgieter¹¹⁰, I.Y. Pozos⁴³, K.K. Pradhan⁴⁷, S.K. Prasad⁴, S. Prasad⁴⁷, R. Preghenella⁵⁰, F. Prino⁵⁵, C.A. Pruneau¹³⁴,

M. Puccio³², S. Pucillo²⁸, S. Pulawski¹¹⁷, L. Quaglia²⁴, A.M.K. Radhakrishnan⁴⁷, S. Ragoni¹⁴, A. Rai¹³⁵, A. Rakotozafindrabe¹²⁷, N. Ramasubramanian¹²⁵, L. Ramello^{130,55}, C.O. Ramírez-Álvarez⁴³, M. Rasa²⁶, S.S. Räsänen⁴², R. Rath⁹⁴, M.P. Rauch²⁰, I. Ravasenga³², M. Razza²⁵, K.F. Read^{84,119}, C. Reckziegel¹⁰⁸, A.R. Redelbach³⁸, K. Redlich^{VII,76}, C.A. Reetz⁹⁴, H.D. Regules-Medel⁴³, A. Rehman²⁰, F. Reidt³², H.A. Reme-Ness³⁷, K. Reygers⁹¹, M. Richter²⁰, A.A. Riedel⁹², W. Riegler³², A.G. Riffero²⁴, M. Rignanese²⁷, C. Ripoli²⁸, C. Ristea⁶², M.V. Rodríguez³², M. Rodríguez Cahuantzi⁴³, K. Røed¹⁹, E. Rogochaya¹³⁹, D. Rohr³², D. Röhrich²⁰, S. Rojas Torres³⁴, P.S. Rokita¹³³, G. Romanenko²⁵, F. Ronchetti³², D. Rosales Herrera⁴³, E.D. Rosas⁶⁴, K. Roslon¹³³, A. Rossi⁵³, A. Roy⁴⁷, S. Roy⁴⁶, N. Rubini⁵⁰, O. Rubza^{I,15}, J.A. Rudolph⁸¹, D. Ruggiano¹³³, R. Rui²³, P.G. Russek², A. Rustamov⁷⁸, A. Rybicki¹⁰³, L.C.V. Ryder¹¹⁴, G. Ryu⁶⁹, J. Ryu¹⁶, W. Rzesza⁹², B. Sabiu⁵⁰, R. Sadek⁷¹, S. Sadhu⁴¹, A. Saha³¹, S. Saha⁷⁷, B. Sahoo⁴⁷, R. Sahoo⁴⁷, D. Sahu⁶⁴, P.K. Sahu⁶⁰, J. Saini¹³², S. Sakai¹²², S. Sambyal⁸⁸, D. Samitz⁷³, I. Sanna³², D. Sarkar⁸⁰, V. Sarritzu²², V.M. Sarti⁹², M.H.P. Sas⁸¹, U. Savino²⁴, S. Sawan⁷⁷, E. Scapparone⁵⁰, J. Schambach⁸⁴, H.S. Scheid³², C. Schiaua⁴⁴, R. Schicker⁹¹, F. Schlepfer^{32,91}, A. Schmah⁹⁴, C. Schmidt⁹⁴, M. Schmidt⁹⁰, J. Schoengarth⁶³, R. Schotter⁷³, A. Schröter³⁸, J. Schukraft³², K. Schweda⁹⁴, G. Scioli²⁵, E. Scopinich⁵⁵, J.E. Seger¹⁴, D. Sekihata¹²¹, M. Selina⁸¹, I. Selyuzhenkov⁹⁴, S. Senyukov¹²⁶, J.J. Seo⁹¹, L. Serkin^{VIII,64}, L. Šerkšnytė³², A. Sevcenco⁶², T.J. Shaba⁶⁷, A. Shabetai⁹⁹, R. Shahoyan³², B. Sharma⁸⁸, D. Sharma⁴⁶, H. Sharma⁵³, M. Sharma⁸⁸, S. Sharma⁸⁸, T. Sharma⁴⁰, U. Sharma⁸⁸, O. Sheibani¹³⁴, K. Shigaki⁸⁹, M. Shimomura⁷⁵, Q. Shou³⁹, S. Siddhanta⁵¹, T. Siemiarczuk⁷⁶, T.F. Silva¹⁰⁶, W.D. Silva¹⁰⁶, D. Silvermyr⁷², T. Simantathammakul¹⁰¹, R. Simeonov³⁵, B. Singh⁴⁶, B. Singh⁸⁸, B. Singh⁹², K. Singh⁴⁷, R. Singh⁷⁷, R. Singh⁵³, S. Singh¹⁵, T. Sinha⁹⁶, B. Sitar¹³, M. Sitta^{130,55}, T.B. Skaali¹⁹, G. Skorodumovs⁹¹, N. Smirnov¹³⁵, K.L. Smith¹⁶, R.J.M. Snellings⁵⁸, E.H. Solheim¹⁹, S. Solokhin⁸¹, C. Sonnabend^{32,94}, J.M. Sonneveld⁸¹, F. Soramel²⁷, A.B. Soto-Hernandez⁸⁵, R. Spijkers⁸¹, C. Sporleder¹¹³, I. Sputowska¹⁰³, J. Staa⁷², J. Stachel⁹¹, L.L. Stahl¹⁰⁶, I. Stan⁶², A.G. Stejskal¹¹⁴, T. Stellhorn¹²³, S.F. Stiefelmaier⁹¹, D. Stocco⁹⁹, I. Storehaug¹⁹, N.J. Strangmann⁶³, P. Stratmann¹²³, S. Strazzi²⁵, A. Sturmiolo^{115,30,52}, Y. Su⁶, A.A.P. Suaide¹⁰⁶, C. Suire¹²⁸, A. Suiu¹⁰⁹, M. Sukhanov¹³⁹, M. Suljic³², V. Sumberia⁸⁸, S. Sumowidagdo⁷⁹, P. Sun¹⁰, N.B. Sundstrom⁵⁸, L.H. Tabares⁷, A. Tabikh⁷⁰, S.F. Taghavi⁹², J. Takahashi¹⁰⁷, M.A. Talamantes Johnson⁴³, G.J. Tambave⁷⁷, Z. Tang¹¹⁶, J. Tanwar⁸⁷, J.D. Tapia Takaki¹¹⁴, N. Tapus¹⁰⁹, L.A. Tarasovicova³⁶, M.G. Tarczila⁴⁴, A. Tauro³², A. Tavira García¹²⁸, G. Tejeda Muñoz⁴³, L. Terlizzi²⁴, C. Terrevoli⁴⁹, D. Thakur⁵⁵, S. Thakur⁴, M. Thogersen¹⁹, D. Thomas¹⁰⁴, A.M. Tieckötter¹²³, N. Tiltmann^{32,123}, A.R. Timmins¹¹², A. Toia⁶³, R. Tokumoto⁸⁹, S. Tomassini²⁵, K. Tomohiro⁸⁹, Q. Tong⁶, V.V. Torres⁹⁹, A. Trifiró^{30,52}, T. Triloki⁹³, A.S. Triolo³², S. Tripathy³², T. Tripathy¹²⁴, S. Trogolo²⁴, V. Trubnikov³, W.H. Trzaska¹¹³, T.P. Trzcinski¹³³, C. Tzolanta¹⁹, R. Tu³⁹, R. Turrisi⁵³, T.S. Tveter¹⁹, K. Ullaland²⁰, B. Ulukutlu⁹², S. Upadhyaya¹⁰³, A. Uras¹²⁵, M. Urioni²³, G.L. Usai²², M. Vaid⁸⁸, M. Vala³⁶, N. Valle⁵⁴, L.V.R. van Doremalen⁵⁸, M. van Leeuwen⁸¹, C.A. van Veen⁹¹, R.J.G. van Weelden⁸¹, D. Varga⁴⁵, Z. Varga¹³⁵, P. Vargas Torres⁶⁴, O. Vázquez Doce⁴⁸, O. Vazquez Rueda¹¹², G. Vecil²³, P. Veen¹²⁷, E. Vercellin²⁴, R. Verma⁴⁶, R. Vértési⁴⁵, M. Verweij⁵⁸, L. Vickovic³³, Z. Vilakazi¹²⁰, A. Villani²³, C.J.D. Villiers⁶⁷, T. Virgili²⁸, M.M.O. Virta⁴², A. Vodopyanov¹³⁹, M.A. Völkl⁹⁷, S.A. Voloshin¹³⁴, G. Volpe³¹, B. von Haller³², I. Vorobyev³², N. Vozniuk¹³⁹, J. Vrláková³⁶, J. Wan³⁹, C. Wang³⁹, D. Wang³⁹, Y. Wang¹¹⁶, Y. Wang³⁹, Y. Wang⁶, Z. Wang³⁹, F. Weiglhofer³², S.C. Wenzel³², J.P. Wessels¹²³, P.K. Wiacek², J. Wiechula⁶³, J. Wikne¹⁹, G. Wilk⁷⁶, J. Wilkinson⁹⁴, G.A. Willems¹²³, N. Wilson¹¹⁵, B. Windelband⁹¹, J. Witte⁹¹, M. Wojnar², C.I. Worek², J.R. Wright¹⁰⁴, C.-T. Wu^{6,27}, W. Wu^{92,39}, Y. Wu¹¹⁶, K. Xiong³⁹, Z. Xiong¹¹⁶, L. Xu^{125,6}, R. Xu⁶, Z. Xue⁷¹, A. Yadav⁴¹, A.K. Yadav¹³², Y. Yamaguchi⁸⁹, S. Yang⁵⁷, S. Yang²⁰, S. Yano⁸⁹, Z. Ye⁷¹, E.R. Yeats¹⁸, J. Yi⁶, R. Yin³⁹, Z. Yin⁶, I.-K. Yoo¹⁶, J.H. Yoon⁵⁷, H. Yu¹², S. Yuan²⁰, A. Yuncu⁹¹, V. Zaccolo²³, C. Zampolli³², F. Zanone⁹¹, N. Zardoshti³², P. Závada⁶¹, B. Zhang⁹¹, C. Zhang¹²⁷, L. Zhang³⁹, M. Zhang^{124,6}, M. Zhang^{27,6}, S. Zhang³⁹, X. Zhang⁶, Y. Zhang¹¹⁶, Y. Zhang¹¹⁶, Z. Zhang⁶, D. Zhou⁶, Y. Zhou⁸⁰, Z. Zhou³⁹, J. Zhu³⁹, S. Zhu^{94,116}, Y. Zhu⁶, A. Zingaretti²⁷, S.C. Zugravel⁵⁵, N. Zurlo^{131,54}

Affiliation Notes

¹ Deceased

- ^{II} Also at: Max-Planck-Institut für Physik, Munich, Germany
- ^{III} Also at: Czech Technical University in Prague (CZ)
- ^{IV} Also at: Instituto de Física da Universidade de São Paulo
- ^V Also at: Dipartimento DET del Politecnico di Torino, Turin, Italy
- ^{VI} Also at: Department of Applied Physics, Aligarh Muslim University, Aligarh, India
- ^{VII} Also at: Institute of Theoretical Physics, University of Wrocław, Poland
- ^{VIII} Also at: Facultad de Ciencias, Universidad Nacional Autónoma de México, Mexico City, Mexico

Collaboration Institutes

- ¹ A.I. Alikhanyan National Science Laboratory (Yerevan Physics Institute) Foundation, Yerevan, Armenia
- ² AGH University of Krakow, Cracow, Poland
- ³ Bogolyubov Institute for Theoretical Physics, National Academy of Sciences of Ukraine, Kyiv, Ukraine
- ⁴ Bose Institute, Department of Physics and Centre for Astroparticle Physics and Space Science (CAPSS), Kolkata, India
- ⁵ California Polytechnic State University, San Luis Obispo, California, United States
- ⁶ Central China Normal University, Wuhan, China
- ⁷ Centro de Aplicaciones Tecnológicas y Desarrollo Nuclear (CEADEN), Havana, Cuba
- ⁸ Centro de Investigación y de Estudios Avanzados (CINVESTAV), Mexico City and Mérida, Mexico
- ⁹ Chicago State University, Chicago, Illinois, United States
- ¹⁰ China Nuclear Data Center, China Institute of Atomic Energy, Beijing, China
- ¹¹ China University of Geosciences, Wuhan, China
- ¹² Chungbuk National University, Cheongju, Republic of Korea
- ¹³ Comenius University Bratislava, Faculty of Mathematics, Physics and Informatics, Bratislava, Slovak Republic
- ¹⁴ Creighton University, Omaha, Nebraska, United States
- ¹⁵ Department of Physics, Aligarh Muslim University, Aligarh, India
- ¹⁶ Department of Physics, Pusan National University, Pusan, Republic of Korea
- ¹⁷ Department of Physics, Sejong University, Seoul, Republic of Korea
- ¹⁸ Department of Physics, University of California, Berkeley, California, United States
- ¹⁹ Department of Physics, University of Oslo, Oslo, Norway
- ²⁰ Department of Physics and Technology, University of Bergen, Bergen, Norway
- ²¹ Dipartimento di Fisica, Università di Pavia, Pavia, Italy
- ²² Dipartimento di Fisica dell'Università and Sezione INFN, Cagliari, Italy
- ²³ Dipartimento di Fisica dell'Università and Sezione INFN, Trieste, Italy
- ²⁴ Dipartimento di Fisica dell'Università and Sezione INFN, Turin, Italy
- ²⁵ Dipartimento di Fisica e Astronomia dell'Università and Sezione INFN, Bologna, Italy
- ²⁶ Dipartimento di Fisica e Astronomia dell'Università and Sezione INFN, Catania, Italy
- ²⁷ Dipartimento di Fisica e Astronomia dell'Università and Sezione INFN, Padova, Italy
- ²⁸ Dipartimento di Fisica 'E.R. Caianiello' dell'Università and Gruppo Collegato INFN, Salerno, Italy
- ²⁹ Dipartimento DISAT del Politecnico and Sezione INFN, Turin, Italy
- ³⁰ Dipartimento di Scienze MIFT, Università di Messina, Messina, Italy
- ³¹ Dipartimento Interateneo di Fisica 'M. Merlin' and Sezione INFN, Bari, Italy
- ³² European Organization for Nuclear Research (CERN), Geneva, Switzerland
- ³³ Faculty of Electrical Engineering, Mechanical Engineering and Naval Architecture, University of Split, Split, Croatia
- ³⁴ Faculty of Nuclear Sciences and Physical Engineering, Czech Technical University in Prague, Prague, Czech Republic
- ³⁵ Faculty of Physics, Sofia University, Sofia, Bulgaria
- ³⁶ Faculty of Science, P.J. Šafárik University, Košice, Slovak Republic
- ³⁷ Faculty of Technology, Environmental and Social Sciences, Bergen, Norway
- ³⁸ Frankfurt Institute for Advanced Studies, Johann Wolfgang Goethe-Universität Frankfurt, Frankfurt, Germany
- ³⁹ Fudan University, Shanghai, China
- ⁴⁰ Gauhati University, Department of Physics, Guwahati, India
- ⁴¹ Helmholtz-Institut für Strahlen- und Kernphysik, Rheinische Friedrich-Wilhelms-Universität Bonn, Bonn, Germany
- ⁴² Helsinki Institute of Physics (HIP), Helsinki, Finland

- 43 High Energy Physics Group, Universidad Autónoma de Puebla, Puebla, Mexico
44 Horia Hulubei National Institute of Physics and Nuclear Engineering, Bucharest, Romania
45 HUN-REN Wigner Research Centre for Physics, Budapest, Hungary
46 Indian Institute of Technology Bombay (IIT), Mumbai, India
47 Indian Institute of Technology Indore, Indore, India
48 INFN, Laboratori Nazionali di Frascati, Frascati, Italy
49 INFN, Sezione di Bari, Bari, Italy
50 INFN, Sezione di Bologna, Bologna, Italy
51 INFN, Sezione di Cagliari, Cagliari, Italy
52 INFN, Sezione di Catania, Catania, Italy
53 INFN, Sezione di Padova, Padova, Italy
54 INFN, Sezione di Pavia, Pavia, Italy
55 INFN, Sezione di Torino, Turin, Italy
56 INFN, Sezione di Trieste, Trieste, Italy
57 Inha University, Incheon, Republic of Korea
58 Institute for Gravitational and Subatomic Physics (GRASP), Utrecht University/Nikhef, Utrecht, Netherlands
59 Institute of Experimental Physics, Slovak Academy of Sciences, Košice, Slovak Republic
60 Institute of Physics, Homi Bhabha National Institute, Bhubaneswar, India
61 Institute of Physics of the Czech Academy of Sciences, Prague, Czech Republic
62 Institute of Space Science (ISS), Bucharest, Romania
63 Institut für Kernphysik, Johann Wolfgang Goethe-Universität Frankfurt, Frankfurt, Germany
64 Instituto de Ciencias Nucleares, Universidad Nacional Autónoma de México, Mexico City, Mexico
65 Instituto de Física, Universidade Federal do Rio Grande do Sul (UFRGS), Porto Alegre, Brazil
66 Instituto de Física, Universidad Nacional Autónoma de México, Mexico City, Mexico
67 iThemba LABS, National Research Foundation, Somerset West, South Africa
68 Jeonbuk National University, Jeonju, Republic of Korea
69 Korea Institute of Science and Technology Information, Daejeon, Republic of Korea
70 Laboratoire de Physique Subatomique et de Cosmologie, Université Grenoble-Alpes, CNRS-IN2P3, Grenoble, France
71 Lawrence Berkeley National Laboratory, Berkeley, California, United States
72 Lund University Department of Physics, Division of Particle Physics, Lund, Sweden
73 Marietta Blau Institute, Vienna, Austria
74 Nagasaki Institute of Applied Science, Nagasaki, Japan
75 Nara Women's University (NWU), Nara, Japan
76 National Centre for Nuclear Research, Warsaw, Poland
77 National Institute of Science Education and Research, Homi Bhabha National Institute, Jatni, India
78 National Nuclear Research Center, Baku, Azerbaijan
79 National Research and Innovation Agency - BRIN, Jakarta, Indonesia
80 Niels Bohr Institute, University of Copenhagen, Copenhagen, Denmark
81 Nikhef, National institute for subatomic physics, Amsterdam, Netherlands
82 Nuclear Physics Group, STFC Daresbury Laboratory, Daresbury, United Kingdom
83 Nuclear Physics Institute of the Czech Academy of Sciences, Husinec-Řež, Czech Republic
84 Oak Ridge National Laboratory, Oak Ridge, Tennessee, United States
85 Ohio State University, Columbus, Ohio, United States
86 Physics department, Faculty of science, University of Zagreb, Zagreb, Croatia
87 Physics Department, Panjab University, Chandigarh, India
88 Physics Department, University of Jammu, Jammu, India
89 Physics Program and International Institute for Sustainability with Knotted Chiral Meta Matter (WPI-SKCM²), Hiroshima University, Hiroshima, Japan
90 Physikalisches Institut, Eberhard-Karls-Universität Tübingen, Tübingen, Germany
91 Physikalisches Institut, Ruprecht-Karls-Universität Heidelberg, Heidelberg, Germany
92 Physik Department, Technische Universität München, Munich, Germany
93 Politecnico di Bari and Sezione INFN, Bari, Italy
94 Research Division and ExtreMe Matter Institute EMMI, GSI Helmholtzzentrum für Schwerionenforschung GmbH, Darmstadt, Germany
95 Saga University, Saga, Japan

- ⁹⁶ Saha Institute of Nuclear Physics, Homi Bhabha National Institute, Kolkata, India
⁹⁷ School of Physics and Astronomy, University of Birmingham, Birmingham, United Kingdom
⁹⁸ Sección Física, Departamento de Ciencias, Pontificia Universidad Católica del Perú, Lima, Peru
⁹⁹ SUBATECH, IMT Atlantique, Nantes Université, CNRS-IN2P3, Nantes, France
¹⁰⁰ Sungkyunkwan University, Suwon City, Republic of Korea
¹⁰¹ Suranaree University of Technology, Nakhon Ratchasima, Thailand
¹⁰² Technical University of Košice, Košice, Slovak Republic
¹⁰³ The Henryk Niewodniczanski Institute of Nuclear Physics, Polish Academy of Sciences, Cracow, Poland
¹⁰⁴ The University of Texas at Austin, Austin, Texas, United States
¹⁰⁵ Universidad Autónoma de Sinaloa, Culiacán, Mexico
¹⁰⁶ Universidade de São Paulo (USP), São Paulo, Brazil
¹⁰⁷ Universidade Estadual de Campinas (UNICAMP), Campinas, Brazil
¹⁰⁸ Universidade Federal do ABC, Santo Andre, Brazil
¹⁰⁹ Universitatea Nationala de Stiinta si Tehnologie Politehnica Bucuresti, Bucharest, Romania
¹¹⁰ University of Cape Town, Cape Town, South Africa
¹¹¹ University of Derby, Derby, United Kingdom
¹¹² University of Houston, Houston, Texas, United States
¹¹³ University of Jyväskylä, Jyväskylä, Finland
¹¹⁴ University of Kansas, Lawrence, Kansas, United States
¹¹⁵ University of Liverpool, Liverpool, United Kingdom
¹¹⁶ University of Science and Technology of China, Hefei, China
¹¹⁷ University of Silesia in Katowice, Katowice, Poland
¹¹⁸ University of South-Eastern Norway, Kongsberg, Norway
¹¹⁹ University of Tennessee, Knoxville, Tennessee, United States
¹²⁰ University of the Witwatersrand, Johannesburg, South Africa
¹²¹ University of Tokyo, Tokyo, Japan
¹²² University of Tsukuba, Tsukuba, Japan
¹²³ Universität Münster, Institut für Kernphysik, Münster, Germany
¹²⁴ Université Clermont Auvergne, CNRS/IN2P3, LPC, Clermont-Ferrand, France
¹²⁵ Université de Lyon, CNRS/IN2P3, Institut de Physique des 2 Infinis de Lyon, Lyon, France
¹²⁶ Université de Strasbourg, CNRS, IPHC UMR 7178, F-67000 Strasbourg, France, Strasbourg, France
¹²⁷ Université Paris-Saclay, Centre d'Etudes de Saclay (CEA), IRFU, Département de Physique Nucléaire (DPhN), Saclay, France
¹²⁸ Université Paris-Saclay, CNRS/IN2P3, IJCLab, Orsay, France
¹²⁹ Università degli Studi di Foggia, Foggia, Italy
¹³⁰ Università del Piemonte Orientale, Vercelli, Italy
¹³¹ Università di Brescia, Brescia, Italy
¹³² Variable Energy Cyclotron Centre, Homi Bhabha National Institute, Kolkata, India
¹³³ Warsaw University of Technology, Warsaw, Poland
¹³⁴ Wayne State University, Detroit, Michigan, United States
¹³⁵ Yale University, New Haven, Connecticut, United States
¹³⁶ Yildiz Technical University, Istanbul, Turkey
¹³⁷ Yonsei University, Seoul, Republic of Korea
¹³⁸ Affiliated with an institute formerly covered by a cooperation agreement with CERN
¹³⁹ Affiliated with an international laboratory covered by a cooperation agreement with CERN.